Effect of the SARS-CoV-2 Delta-associated G15U mutation on the s2m element dimerization and its interactions with miR-1307-3p

CAYLEE L. CUNNINGHAM,[1] CALEB J. FRYE,[1] JOSEPH A. MAKOWSKI,[1] ADAM H. KENSINGER,[1] MORGAN SHINE,[2] ELLA J. MILBACK,[1] PATRICK E. LACKEY,[2] JEFFREY D. EVANSECK,[1] and MIHAELA-RITA MIHAILESCU[1]

[1]Department of Chemistry and Biochemistry, Duquesne University, Pittsburgh, Pennsylvania 15282, USA
[2]Department of Biochemistry and Chemistry, Westminster College, New Wilmington, Pennsylvania 16172, USA

ABSTRACT

The s2m, a highly conserved 41-nt hairpin structure in the SARS-CoV-2 genome, serves as an attractive therapeutic target that may have important roles in the virus life cycle or interactions with the host. However, the conserved s2m in Delta SARS-CoV-2, a previously dominant variant characterized by high infectivity and disease severity, has received relatively less attention than that of the original SARS-CoV-2 virus. The focus of this work is to identify and define the s2m changes between Delta and SARS-CoV-2 and the subsequent impact of those changes upon the s2m dimerization and interactions with the host microRNA miR-1307-3p. Bioinformatics analysis of the GISAID database targeting the s2m element reveals a >99% correlation of a single nucleotide mutation at the 15th position (G15U) in Delta SARS-CoV-2. Based on ^{1}H NMR spectroscopy assignments comparing the imino proton resonance region of s2m and the s2m G15U at 19°C, we show that the U15–A29 base pair closes, resulting in a stabilization of the upper stem without overall secondary structure deviation. Increased stability of the upper stem did not affect the chaperone activity of the viral N protein, as it was still able to convert the kissing dimers formed by s2m G15U into a stable duplex conformation, consistent with the s2m reference. However, we show that the s2m G15U mutation drastically impacts the binding of host miR-1307-3p. These findings demonstrate that the observed G15U mutation alters the secondary structure of s2m with subsequent impact on viral binding of host miR-1307-3p, with potential consequences on immune responses.

Keywords: SARS-CoV-2 Delta; dimerization; kissing complex; miR-1307-3p; s2m

INTRODUCTION

The effects of the coronavirus disease 2019 (COVID-19) pandemic continue to impact the world, as the virus responsible for the outbreak, severe acute respiratory syndrome coronavirus 2 (SARS-CoV-2), continues to acquire advantageous mutations, resulting in new viral variants. To date, SARS-CoV-2 has resulted in over 768 million identified cases and 6.9 million deaths worldwide, with countless others going unreported, underscoring the need to characterize the viral life cycle and interactions with the host so that future pandemics may be thwarted (CDC 2020b). Although some variants of SARS-CoV-2 were short-lived, several created new waves of infections. These variants exhibited heightened levels of "immune escape" as well as changes in symptom severity (CDC 2020a,b; WHO Coronavirus Dashboard, https://covid19.who.int). One of these variants, identified as the Delta variant, originated in India with the earliest documented case in October 2020 (Duong 2021). Delta was subsequently declared a variant of concern (VOC) by the World Health Organization in May 2021 and became the dominant variant of the virus soon after. In November 2021, Delta cases began decreasing as a new prominent variant, Omicron, emerged (CDC 2020b; Yaniv et al. 2022; Tracking SARS-CoV-2 variants, https://www.who.int/activities/tracking-SARS-CoV-2-variants). Omicron was quickly declared a VOC on November 26, 2021 and has since mutated into several sublineages, with recent work suggesting that Omicron gained several mutations throughout its genome, aiding in transmissibility (CDC 2020a; Jung

Corresponding author: mihailescum@duq.edu
Article is online at http://www.rnajournal.org/cgi/doi/10.1261/rna.079627.123.

et al. 2022; Meng et al. 2022). As new major SARS-CoV-2 variants and sublineages emerged, their transmissibility increased while the disease severity fluctuated, suggesting the virus is adapting to increase its viral spread and longevity (CDC 2022). Although Omicron is presently the most prevalent variant, it was not able to fully out-compete its VOC predecessor, as Delta cases collected as late as April and May 2023 are still reported in the various parts of the world (e.g., EPI_ISL_17701782 in the USA; EPI_ISL_17780726 in Italy; EPI_ISL_17523131 in Ukraine). This is unlike the eradication of the previous Gamma and Beta variants, making the Delta variant even more interesting to study due to its viability (Yaniv et al. 2022; Caserta et al. 2023).

SARS-CoV-2 variants are classified by advantageous mutations to the spike (S) protein, particularly those which increase binding affinity to the angiotensin-converting enzyme 2 (ACE2) receptor, the viral entry point into the host cell (Yan et al. 2020). However, in addition to open reading frames, the SARS-CoV-2 genome contains both 5′- and 3′-untranslated regions (UTRs) that harbor highly conserved structures that play vital roles in the replication of both the genomic and subgenomic RNAs (Lulla et al. 2021; Malone et al. 2022). In addition to differences in the S protein, mutations exist within the Delta variant's 5′- and 3′-UTRs. We focused on the 3′-UTR of SARS-CoV-2 as it contains a 41 nt highly conserved secondary structure termed the stem–loop II motif (s2m) element (Fig. 1, bottom; Jonassen 2008; Tengs et al. 2013; Tengs and Jonassen 2016; Gilbert and Tengs 2021). Previous research has demonstrated that in addition to coronaviruses, this motif is present in three other single-stranded viral families, Astroviridae, Caliciviridae and Picornaviridae (Tengs et al. 2013; Tengs and Jonassen 2016). Although the exact roles of this element have not been elucidated, the high level of s2m sequence conservation within the hyper variable region of the 3′-UTR led to the belief that it is beneficial to the virus (Gilbert and Tengs 2021). Some of the suggested functions of the s2m include host microRNA (miR) hijacking, host protein hijacking, and involvement in viral recombination events (Robertson et al. 2005; Yeh and Contreras 2020). We previously reported that, through the presence of a palindromic sequence at the terminal loop, a kissing dimer (KD) structure forms between two s2m elements which is converted to an extended duplex (ED) structure by the viral nucleocapsid (N) protein (Fig. 2; Imperatore et al. 2022). From this observation, we proposed that this process could be important in recombination and template switching, leading to the adaptation of new mutations to come (Muriaux et al. 1996; Shetty et al. 2010; Imperatore et al. 2022). Additionally, we have shown that the s2m is able to bind up to two copies of the host miR-1307-3p (Imperatore et al. 2022). The binding of miRs to the UTR can be beneficial to enhance viral replication; however, this interaction may also be a part of the host's immune response to the viral infection (Arisan et al. 2020; Balmeh et al. 2020).

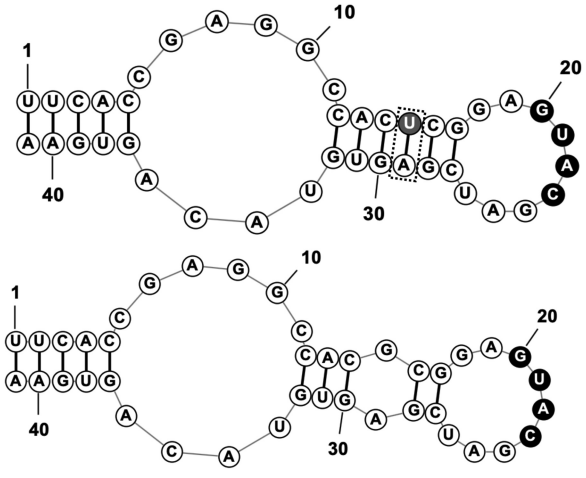

FIGURE 1. RNAStructure representation of the secondary structures of the SARS-CoV-2 s2m reference (bottom) and G15U mutation (top). The closing of the U15 and A29 base pair is indicated in the top s2m G15U by the dashed box.

Notably, only a 2-nt difference exists between the s2m of SARS-CoV-2 and SARS-CoV, the related virus responsible for the 2002–2003 outbreak of "SARS." One of those mutations, G > U at position 31 (G31U) of the s2m (29,758 in the reference SARS-CoV-2 genome, EPI_ISL_402123), has previously been conserved as a G in all other reported s2m elements, and our earlier study revealed that G31U is the causative mutation between differences in dimerization properties in SARS-CoV-2 s2m and SARS-CoV s2m, as well as in miR-1307-3p binding (Zhao et al. 2020; Imperatore et al. 2022). Moreover, our molecular dynamics (MD) simulation study showed that these dimerization differences are likely caused by increases in structural flexibility of the terminal loop in SARS-CoV-2 s2m compared to the rigid GNRA-like pentaloop motif found in the SARS-CoV s2m (Kensinger et al. 2022). In SARS-CoV-2 s2m, an expansion to a "nonaloop" was computed to confer an entropic penalty, potentially explaining the reduction in kissing complex formation, the intermediate step in duplex formation (Kensinger et al. 2022).

Knowing the drastic impact of a single nucleotide mutation on the structure of SARS-CoV-2 s2m, we conducted a bioinformatics analysis ranging from April 2020 to October 2021 to identify new mutations within s2m in SARS-CoV-2 emerging strains. For the Delta variant, we identified a G > U mutation at position 29,742 of the s2m (position 15 within the 41 nt of s2m, hence named here s2m G15U) (Fig. 1, top) that first appeared in January 2020. The results of this analysis revealed a strong correlation between the s2m G15U and the Delta variant of SARS-CoV-2, highlighting a potential advantage conferred by the G15U mutation.

Recent evidence suggests that SARS-CoV-2 is evolving to evade the host immune response in vaccinated individuals, which makes studying the s2m and other structurally

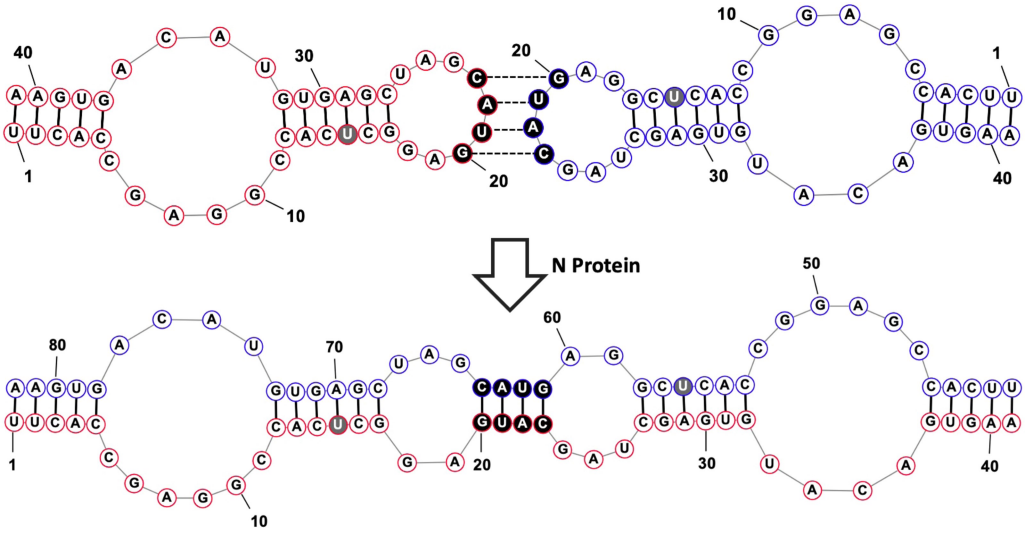

FIGURE 2. RNAStructure depiction of two s2m G15U elements (shown in red and blue for clarity) forming a KD structure through their palindrom-ic sequences, GUAC (filled circles). The N protein then acts as a chaperone to convert the KD intermediate to an ED, a more stable structure. The G15U mutation in the upper stem is highlighted by the filled circle.

conserved elements crucial, in addition to the S protein (Farinholt et al. 2021; Andrews et al. 2022; Telenti et al. 2022; Carabelli et al. 2023; Markov et al. 2023). Thus, in this work, we studied the dimerization properties of the s2m G15U and analyzed its interactions with the human miR-1307-3p, further expanding our breadth of knowledge surrounding s2m (Chan et al. 2020; Alam and Lipovich 2021). A better understanding of the role of conserved RNA structures and how interactions with host RNAs mediate their function will allow us to be better prepared for future variants, especially when considering the increased transmissibility and illness severity caused by the prevalent SARS-CoV-2 Delta variant (Liu and Rocklöv 2021; Luo et al. 2021).

RESULTS AND DISCUSSION

The SARS-CoV-2 Delta variant s2m acquired the G > U mutation at position 15

We performed a bioinformatics analysis to monitor sequence mutants of the SARS-CoV-2 s2m in cases worldwide, specifically targeting India, the United Kingdom, and the United States, three countries which reported a significant number of SARS-CoV-2 sequences to the Global Initiative on Sharing All Influenza Data (GISAID) database (Elbe and Buckland-Merrett 2017). For this mutational analysis, we used a custom R script that extracted and aligned the s2m sequences in all collected SARS-CoV-2 cases (Frye et al. 2023). Our bioinformatics analysis, which sampled SARS-CoV-2 sequences from April 2020 to October 2021, aligned and analyzed a total of 2,034,376 reported sequences to the GISAID database. A total 1980 sequences (0.097%) were removed due to insertions which disrupt the alignment. From this data set, we identified a G to U mutation at position 15 of the s2m, denoted as s2m G15U (Fig. 1, top). The earliest observation of this s2m mutation was in April 2020, within the United Kingdom and the United States, at 0.23% prevalence. While the s2m G15U prevalence remained low for the majority of 2020, we observed an increase in s2m G15U prevalence in April 2021 and May 2021 in the United Kingdom and the United States, respectively (Fig. 3A, orange triangle and blue circle, dashed lines). Interestingly, this increase was concurrent with the rise of the SARS-CoV-2 Delta variant (PANGO lineages B.1.617.2 + AY.*) (Fig. 3A, orange and blue, solid lines). The presence of the s2m G15U rose from 0.23% in March 2021 to a 95.97% plateau in June 2021 in the United Kingdom, and from 0.82% in April 2021 to a 92.40% plateau in July 2021 in the United States. This was simultaneous with the increase in the Delta variant, which rose from 2.03% in March 2021 to 95.68% in June 2021 in the United Kingdom, and from 0.62% in April 2021 to 92.86% in July 2021 in the United States. We determined that the s2m G15U and Delta prevalence maintained an average Pearson's correlation coefficient (R) of 0.9999 for both the United Kingdom and the United States from April 2020 through October 2021, spanning the range of our entire bioinformatics analysis (Supplemental Fig. 1A,B). Additionally, as a control, we studied the Alpha variant (PANGO lineages B.1.1.7 + Q.*) of SARS-CoV-2 and found that only 0.30% of Alpha sequences from November 2020 to August 2021, when this variant was dominant, contained the s2m G15U (Supplemental Fig. 2). This shows that the s2m G15U mutant, while occurring in Alpha at low prevalence, did not rise in prevalence as it had in the Delta variant.

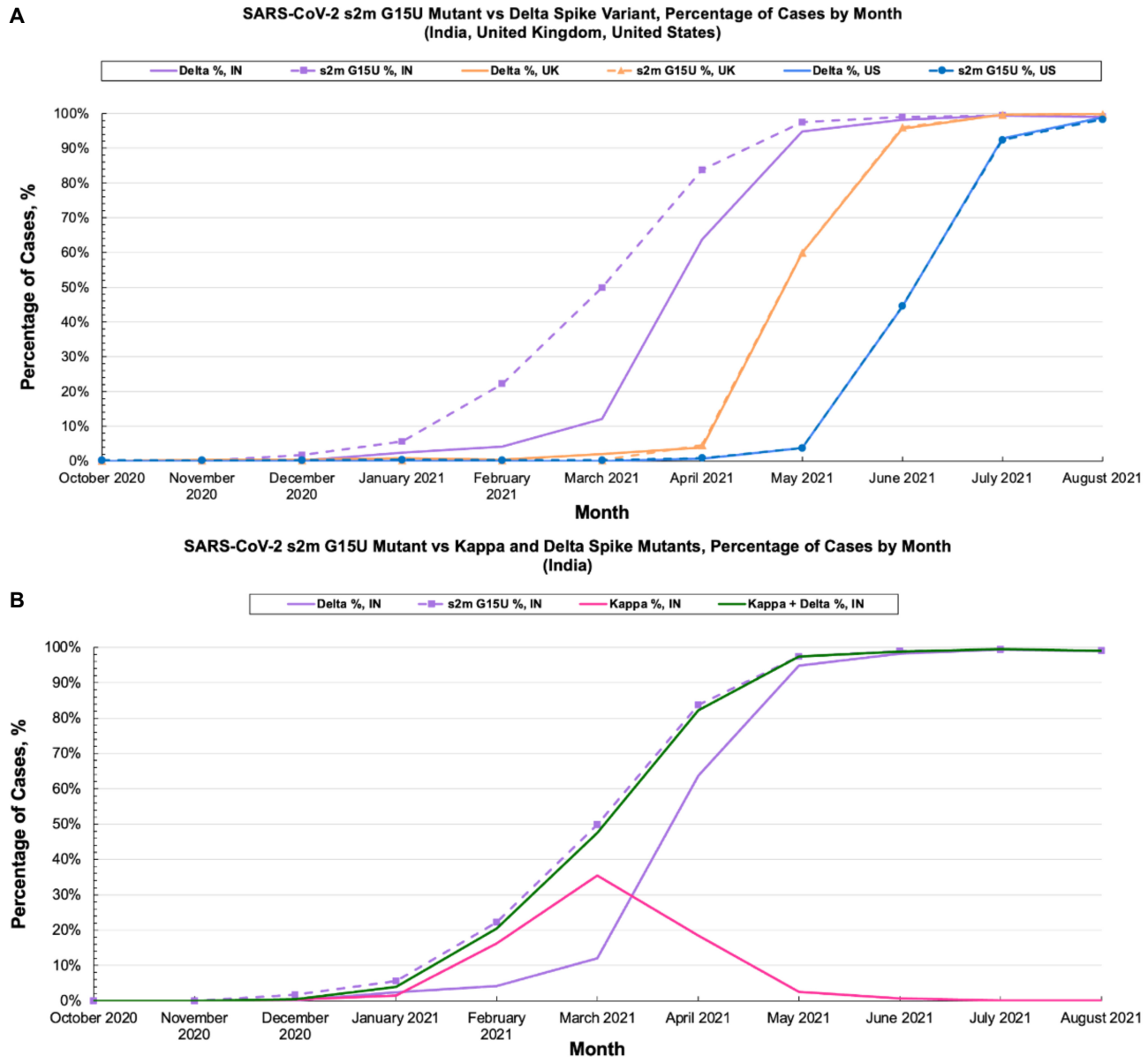

FIGURE 3. (A) Prevalence of the s2m G15U mutation (dashed) and Delta variant (solid) within total reported SARS-CoV-2 cases in the United States (blue), United Kingdom (orange), and India (purple). (B) The s2m G15U mutant (purple dashed line, square markers) rose in prevalence before the rise of the Delta variant (purple solid line). Kappa (pink solid line) was also found to maintain the s2m G15U mutation and comprised of most cases within India that were not accounted for with Delta. The combination of the Kappa and Delta variants' prevalence (green solid line) is tightly correlated with the s2m G15U mutant, mirroring trends later observed as Delta spread worldwide.

While the s2m G15U mutation and Delta variant show a strong positive correlation in prevalence throughout the spread of Delta worldwide, we noted a chronological discrepancy in the s2m G15U and Delta prevalence in India from November 2020 to March 2021, in which the s2m G15U had a noticeable difference in correlation from Delta (Fig. 3A, purple dashed square and solid lines). This difference is of particular interest given that the Delta variant originated in India. Here, the s2m G15U mutant increased significantly from 1.74% in December 2020 to 97.46% by May 2021, with the largest deviation between s2m G15U and Delta in March 2021, as the Delta variant comprised of only 12.06% of submitted cases compared to the 49.87% of s2m G15U. However, through May 2021, both data sets converged as they reached 94.86% and 97.46% for Delta and s2m G15U, respectively. Analysis of these two data sets revealed R = 0.96619 (Supplemental Fig. 1C, green), indicating a positive correlation with greater deviation compared to prior data sets. In efforts to determine the cause of this discrepancy between s2m G15U and Delta, we screened all Delta cases for the percentage of s2m G15U containing sequences and found that the Delta variant was

comprised of 99.32% s2m G15U (Supplemental Fig. 3, blue dashed line). We also analyzed India for other dominant VOCs which may contain the s2m G15U and noted that the Delta variant arose concurrently with a sister variant, Kappa (PANGO lineage B.1.617.1), and found that the s2m G15U is present in 99.05% of all submitted Kappa cases (Supplemental Fig. 3). This finding indicated that Kappa had accounted for a majority of the s2m G15U cases that are not observed within Delta sequences. Combination of the Kappa and Delta prevalence, when plotted against s2m G15U, revealed R = 0.9997 (Supplemental Fig. 1C, purple), indicating a strong positive correlation between the rise in s2m G15U and overall combined incidence of the Kappa and Delta variants. Thus, we attributed the rise of the s2m G15U to a concurrent increase in Kappa and Delta cases. It is to be noted, however, that the Kappa variant was subsequently outcompeted by Delta in March 2021 (Fig. 3B, purple and pink lines), attributed to Delta's increased ACE2 binding affinity and antibody escape (Kannan et al. 2021; Tian et al. 2021; Liu et al. 2022). This trend continues following the drop in Kappa prevalence, in which the combined Kappa and Delta variant prevalence maintains its high correlation with the s2m G15U mutant (Fig. 3B, purple dashed line and green solid line).

The strong positive correlation between the s2m G15U and the Delta variant through its rise in India, and eventual spread worldwide, indicates that the s2m G15U rose in tandem with Delta and was found to be in an average of 99.32% of all Delta sequences. Thus, the presence of s2m G15U in such vast number of Delta SARS-CoV-2 cases and the high conservancy and predicted roles of the s2m in the viral life cycle, warranted its further characterization.

S2m G15U secondary structure characterization

To evaluate the effect of the G15U mutation on the secondary structure of the s2m, we utilized ^{1}H NMR spectroscopy, comparing the imino proton resonance region for the s2m and s2m G15U at 19°C. The SARS-CoV-2 s2m imino proton resonances were previously assigned and thus served as a baseline for our work (Wacker et al. 2020; Imperatore et al. 2022). The previously assigned imino protons corresponding to base pairs in the s2m lower stem (13.19 ppm—G37, 13.42 ppm—U38, and 11.62 ppm—G39) are identical between the two spectra (Fig. 4A). This indicates that the s2m G15U lower stem is not perturbed, consistent with the predicted secondary structures of s2m reference and s2m G15U (Fig. 1). Similarly, the resonance previously assigned to the U31 imino proton has the same chemical shift (13.93 ppm) in the spectrum for the s2m and s2m G15U. We used ^{1}H–^{1}H NOESY NMR spectroscopy on s2m G15U at 19°C to confirm these assignments and assign the remaining imino proton resonances which differ in chemical shift between the s2m reference and s2m G15U. As expected, the resonances assigned to U31 and U38 imino protons (13.93 ppm and 13.42 ppm) have a strong NOE with the H2 of the corresponding adenines they are base paired with (A13 H2 at 7.23 ppm for U31 NH and A4 H2 at 7.18 ppm for U38 NH) (Fig. 4B). In addition, the resonance at 13.66 ppm gives a single strong NOE at 7.39 ppm, a signature of an A–U base pair, allowing us to assign it to the U15 imino proton (Fig. 4B). This result confirms that the G15U mutation closes the base pair U15–A29, as predicted for the s2m G15U secondary structure (Fig. 1, top). Based on its neighboring base pairs, the U31 imino should give rise to NOEs with the G30 and G32 imino protons, and indeed, two cross peaks are observable, at 13.5 ppm and at 11.76 ppm, for the U31 imino proton resonance at 13.93 ppm. Based on its neighboring base pairs, the U15 imino proton should give rise to two NOEs: with the imino protons of G30 and G28. We only observe one clear NOE at 13.5 ppm from the U15 imino proton at 13.66 ppm. Since the imino at 13.5 ppm gives NOEs to both the U31 imino and the U15 imino, we unambiguously assign it to the G30 imino, as this is the only imino proton in the proximity of both U31 and U15 imino protons. Then, by exclusion, the second NOE observed for the U31 imino (13.93 ppm; 11.76 ppm) leads to the assignment of the resonance at 11.76 ppm to the G32 imino proton. This assignment is also supported by the observed NOE between the G32 imino at 11.76 ppm and the A13 H2 at 7.23 ppm. We also observed NOEs between the imino protons of U38 and G37 (13.42 ppm; 13.19 ppm), as well as between the imino of G37 and the A4 H2 at 7.18 ppm, confirming their previous assignment (Fig. 4C; Wacker et al. 2020; Imperatore et al. 2022). A weak NOE is also observed between the imino of G39 at 11.62 ppm and the A4 H2 at 7.18 ppm, confirming the G39 imino assignment (Fig. 4B). Finally, there are two remaining imino proton resonances at 12.03 ppm and 12.7 ppm, which do not give rise to NOEs that would allow us to unambiguously assign them to G28 and G17 iminos. The imino proton resonances of U1 and U2 are not visible in either spectrum due to the dynamic nature of these end base pairs (Imperatore et al. 2022). Based on these assignments we conclude that aside from the obvious mutation which closes the U15–A29 base pair, the s2m G15U secondary structure does not deviate far from that of the s2m.

To further characterize the effect this newly formed base pair has on the stability of the s2m, we performed UV thermal denaturation experiments on s2m G15U and s2m, monitoring the absorbance changes at 260 nm (Fig. 5). The melting temperature, T_m, of each structure was determined from the first derivative plots (Supplemental Fig. 4) to be 44°C and 47°C for the s2m and s2m G15U, respectively. This indicated that, as expected, the closing of the U15–A29 base pair in the s2m G15U upper stem increases the overall stability of the s2m G15U (Figs. 1, 5), which may have implications for the virus' ability to dimerize and form ED structures. In our previous work, we established that the s2m elements of SARS-CoV and SARS-CoV-2 have different dimerization

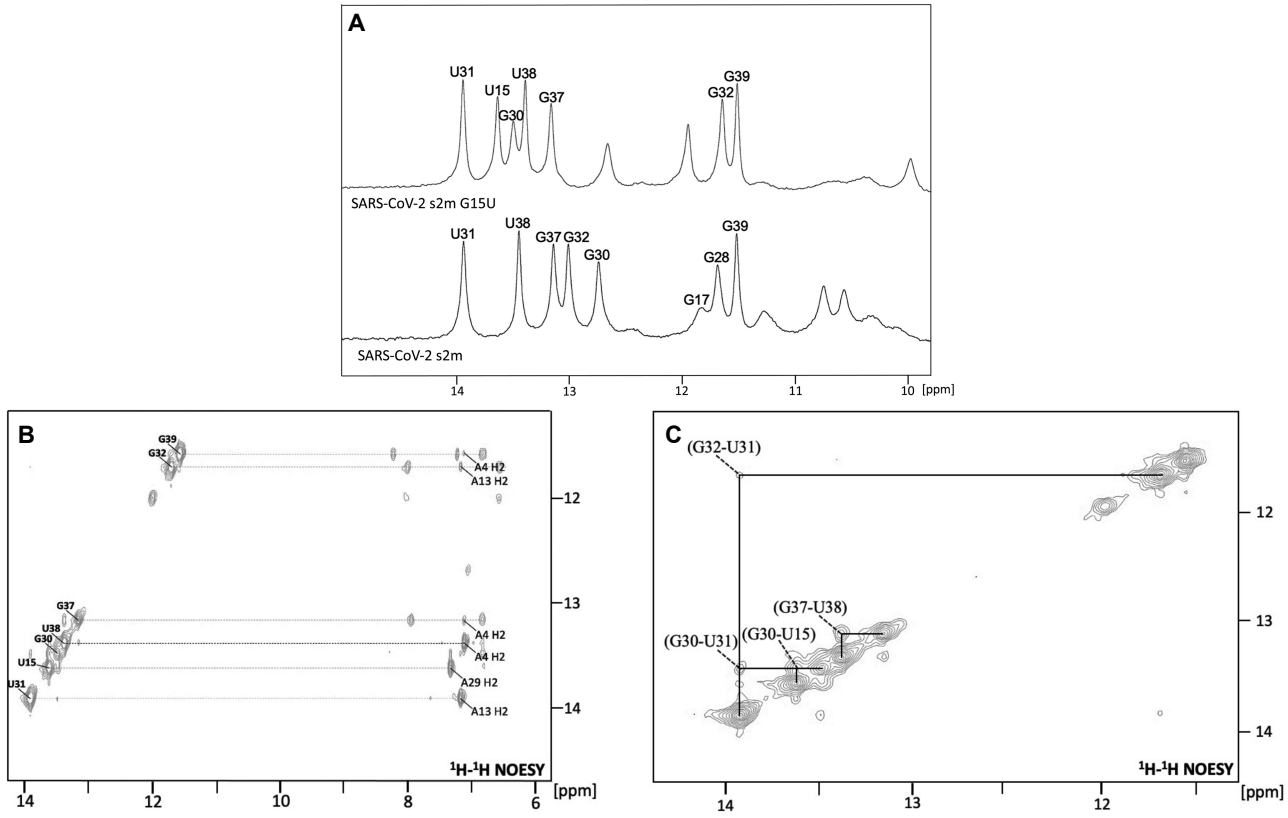

FIGURE 4. (A) One-dimensional ^{1}H NMR spectroscopy of the SARS-CoV-2 s2m G15U (top) and SARS-CoV-2 s2m reference (bottom). The labeled resonances were assigned previously for the s2m reference and in the current work for s2m G15U (Wacker et al. 2020; Imperatore et al. 2022). (B) ^{1}H–^{1}H NOESY spectra of the imino proton resonances of s2m G15U with labeled NOEs between base paired U imino and A H2 and between G imino protons and neighboring A H2. (C) ^{1}H–^{1}H NOESY spectra of the imino proton resonances for the s2m G15U with labeled NOE between neighboring intrastrand and interstrand Gs and Us.

abilities and determined that this is due to the presence of a single nucleotide mutation in s2m G31U located in the s2m upper stem (Imperatore et al. 2022). Such dimerization events in viruses have been shown as critical for genome packaging, inducing conformational changes for translational regulation, reverse transcription processes, as well as being important for genetic recombination (Berkhout and van Wamel 1996; Mikkelsen et al. 2000; Aagaard et al. 2004; Moore et al. 2009; Tengs et al. 2013; Terada et al. 2014). Therefore, next we evaluated the effect of the single nucleotide mutation, the G15U, on the Delta SARS-CoV-2 s2m dimerization.

Characterization of the SARS-CoV-2 s2m G15U dimerization

Our previous work established the presence of a 4 nt palindromic "GUAC" sequence within the terminal loop of the s2m element that participates in loop–loop kissing dimerization (Imperatore et al. 2022). These KD structures are formed through base-pairing between two RNA hairpin loops that contain complementary unpaired nucleotides. Kissing dimers forming with palindromic sequences have been previously reported in other viral systems to be essential for template switching and recombination, a process important for repairing genetic mistakes and increasing diversity within the virus, which is critical for the evolution of new viral strains (Mikkelsen et al. 2000; Andersen et al. 2003). These KDs can then be converted to a thermodynamically stable ED structure through the chaperone activity of the capsid protein when in the context of the entire viral genome (Fig. 2). However, in vitro, short isolated KDs have been reported to form ED conformations spontaneously, such as in hepatitis C virus (HCV) and human immunodeficiency virus (HIV-1) (Muriaux et al. 1996; Mihailescu and Marino 2004; Shetty et al. 2010). In the case of HIV-1, recombination events have led to high rates of immune escape and drug resistance. Thus, given the potential of s2m to be involved in recombination events it is important to determine if the G15U mutation affects its dimerization, as SARS-CoV-2 is still developing new variants (Morris et al. 1999; Rambaut et al. 2004; Dubois et al. 2018).

Therefore, to analyze the G15U mutation's effect upon dimerization of the SARS-CoV-2 s2m, we used TBE/TBM nondenaturing gel electrophoresis, a method used previously in various viral systems to distinguish between KD

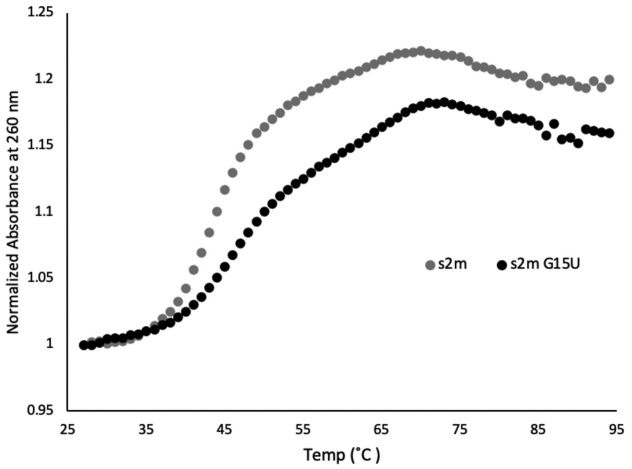

FIGURE 5. UV thermal denaturation of the s2m and s2m G15U at 1 µM in 10 mM cacodylic acid pH 6.5 and absence of $MgCl_2$. The melting temperatures, T_m, were 44°C and 47°C for the s2m reference and s2m G15U, respectively.

versus duplex conformations of dimer initiation sites (Berkhout et al. 2002; Li et al. 2006; Sun et al. 2007; Kenyon et al. 2013). Conditions which maintain $MgCl_2$ concentrations (TBM) stabilize the formation of the KD; however, upon chelation of the Mg^{2+} ions by EDTA in TBE, the KD dissociates, whereas the duplex conformation, which does not require Mg^{2+} ions for stability, is retained. When $MgCl_2$ is retained in the TBM gel, a prominent monomer band (indicated by M) is present for both the s2m and s2m G15U (Fig. 6, right, arrows 1 and 1′). There are two dimer bands present for the s2m reference (Fig. 6, right, arrows 2 and 3), and a single faint dimer band is present for s2m G15U (Fig. 6, right, arrow 3). Our previous report has established that these two upper bands in the s2m reference (Fig. 6, right, arrows 2 and 3) correspond to a KD and ED, respectively (Imperatore et al. 2022). Although both the KD and ED conformations contain the same number of nucleotides, their migration patterns can differ in native gels as these separate RNAs based on both size and shape. Duplex structures are linear, whereas KDs can be present in either a bent or linear state. This would give rise to a different shape that may affect the migration pattern, explaining the difference in the two bands (Ennifar et al. 1999; Rist and Marino 2002). Although unlikely in the context of the entire genome, when the s2m is isolated in its 41 nt state, spontaneous conversion to an ED structure is possible and has been reported in studies involving isolated dimerization initiation sites in other viruses (Muriaux et al. 1996; Mihailescu and Marino 2004; Shetty et al. 2010). Similarly, it is interesting to note that, despite having the same size, the monomer bands for the s2m reference and s2m G15U migrate differently in the TBM gel (Fig. 6, right, arrows 1 and 1′), suggesting that they have different monomer conformations in the presence of $MgCl_2$. Our MD simulations for the s2m revealed that it has a kinked 3D structure; however, the additional U15–A29 base pair in the upper stem of s2m G15U results in a linear structure that lacks the L-shaped kink, rationalizing the increased migration of s2m G15U through the TBM gel as compared to the original s2m form (Kensinger et al. 2022; Makowski et al. 2023). Thus, we cannot determine if the single dimer band observed for the s2m G15U in the TBM gel (Fig. 6, right, arrow 3) originates from a mixture of linear KD and duplex conformations which will migrate at the same position, or from the duplex conformation formed spontaneously from an unstable KD during incubation and migration through the gel (Shetty et al. 2010).

In the TBE gel, after an hour incubation with $MgCl_2$, a prominent monomer s2m band exists for both the s2m reference and the s2m G15U mutant (Fig. 6, left, arrow 1). We also observed faint monomer bands marked by (⍰) originating from degradation products. There are also faint dimer bands present in the TBE gel, which likely originate from the duplex conformations of the intact s2m elements and of its minor degradation products (see below). It is important to note that the TBM gel was run for 4 h in the presence of $MgCl_2$, as opposed to the TBE gel that was run for 2 h, allowing more time for spontaneous conversion of the s2m KD to the duplex conformation, and hence, there is a more prominent duplex band in the TBM gel (Fig. 6, right, arrow 3), as compared to the TBE gel.

However, in the context of the full virus, this conversion from the KD to the ED conformation would not occur spontaneously and would instead require the assistance of the N protein's chaperone activity to facilitate the transition. This process is dependent on the overall stability of the s2m element as base pairs in each monomer will have to be broken, disrupting the monomeric hairpin structure. In coronaviruses, the N protein is responsible for packaging the RNA into ribonucleoprotein complexes to form the mature virion prior to being exported from the host cell (Zúñiga et al. 2007; Aduri et al. 2013). Our previous work has shown that the SARS-CoV-2 N protein selectively acts as a molecular chaperone to convert the s2m KD structure to the stable duplex by a similar mechanism observed for the dimer initiation sites of HIV-1 and HCV (Rist and Marino 2002; Shetty et al. 2010; Shimakami et al. 2012; Imperatore et al. 2022). In HIV-1, a retrovirus, dimerization of the RNA is important for the packaging of two copies of the genome in the mature virion (Dubois et al. 2018). In HCV, a single-stranded RNA virus, this dimerization is suggested to be a regulator of RNA replication and viral genome packaging (Shetty et al. 2010). Additionally, the dimer initiation sites in HIV-1, HCV, and in the murine leukemia virus have been proposed to be implicated in recombination events (Torrent et al. 1994; Greatorex 2004; Masante et al. 2015). We proposed previously that the s2m dimerization mediated by the viral N protein may

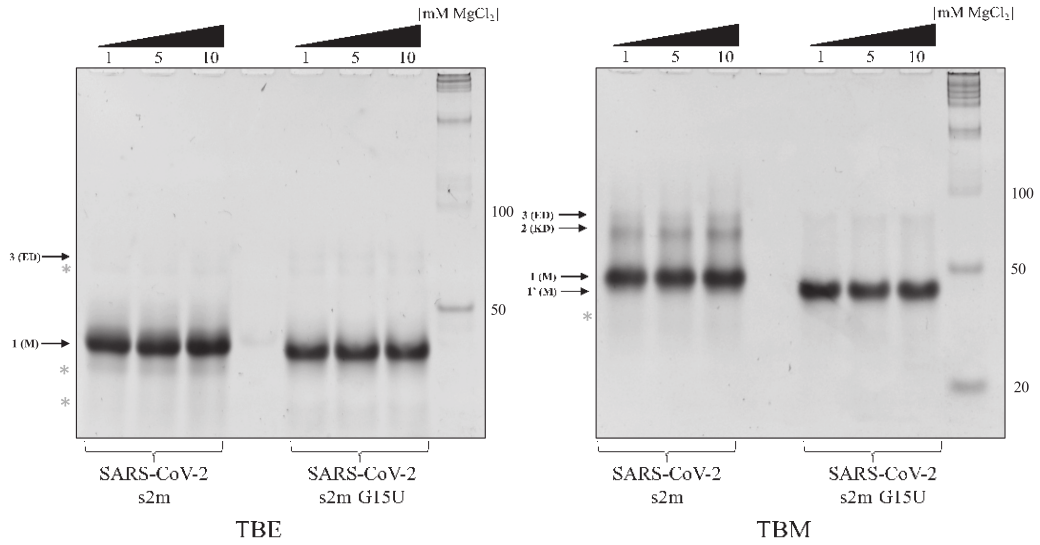

FIGURE 6. TBE (left) and TBM (right) gel nondenaturing electrophoresis analysis of the SARS-CoV-2 s2m reference and the s2m G15U. The two s2m elements were compared using Mg^{2+} dependence where 1 µM RNA was incubated in the presence of 1, 5, or 10 mM $MgCl_2$ for 1 h, then split between two gels—TBE which chelated the Mg^{2+} ions, and TBM that maintained the Mg content. In the TBE, both s2m elements prefer their monomeric (M) states (left, arrow 1). In TBM, the monomeric states are still preferred (right, arrows 1 and 1′). Different migration patterns may be observed due to different shapes of the s2ms, as described in the text. Arrows 2 and 3 indicate the KD and ED, respectively. Degradation products are noted with (*).

facilitate SARS-CoV-2 recombination; thus, here we investigated if the G15U mutation affects the s2m dimerization properties (Imperatore et al. 2022).

To test the chaperone ability of the N protein to convert the s2m G15U to the duplex structure, as compared to the s2m reference, a 1 µM s2m RNA sample was incubated with 1 mM $MgCl_2$ for 30 min, followed by the addition of 2 µM N protein for an additional 30 min. After the incubation with the N or control proteins, proteinase K was added to degrade the proteins prior to loading the samples on the TBE and TBM gels. As demonstrated previously, in TBM both the s2m reference and s2m G15U preferred their monomeric states (Fig. 7, right, arrows 1 and 1′) in the absence of the N protein; however, in the presence of the N protein the two upper bands in the s2m reference became more prominent (Fig. 7, right, arrows 2 and 3; Imperatore et al. 2022). Similarly, the dimer band of s2m G15U, which was barely visible on its own, becomes clear in the presence of the N protein (Fig. 7, right, arrow 3). As discussed above, we cannot distinguish if the s2m G15U KD is unstable (hence the dimer band indicated by arrow 2 is absent in s2m G15U) or if it is a linear structure that migrates at the same position with the duplex conformation. To try to distinguish between these two conformations, we have performed similar experiments incubating the samples with the N protein for times ranging between 1 and 30 min but did not observe any differences in the formation of the dimer band in s2m G15U (data not shown). The TBE/TBM native PAGE method is limited in that it does not allow us to access shorter incubation times with the N protein where we could potentially observe differences in the dimerization of s2m G15U by being able to distinguish between the KD and the ED conformations. When the Mg^{2+} ions are chelated in the TBE gel, a prominent dimer band remains for both s2m and s2m G15U that were incubated with the N protein (Fig. 7, left, arrow 3), indicating that the N protein facilitates the conversion to the duplex conformation in both samples. Note that the faint dimer bands marked by (*) do not line up with the main duplex bands (Fig. 7, left, arrow 3), indicating that they originate from the dimerization of the degradation products. The addition of the P protein or bovine serum albumin (BSA) to the sample had no effect, validating the specificity of the N protein as a molecular chaperone.

Based on these results, we conclude that while the s2m and s2m G15U are converted by the N protein to the duplex conformation, the s2m G15U KD conformation is either not as stable or forms a different conformation than the s2m KD. Specifically, the absence of an s2m G15U KD band at the same position observed for the s2m KD (Fig. 7, right, arrow 2) indicates that the s2m G15U KD could be linear, migrating at the same position with the linear duplex conformation, different than the KD structure of the s2m. Alternately, this could indicate that the s2m G15U KD is able to convert spontaneously to the duplex conformation in the absence of the N protein more efficiently than the s2m; however, considering that the s2m G15U upper stem is more stable and must be opened during this conversion, this scenario is less likely. A difference in KD conformation is more probable as the monomers of these two s2m elements have a different shape based on their different migration in the TBM gel

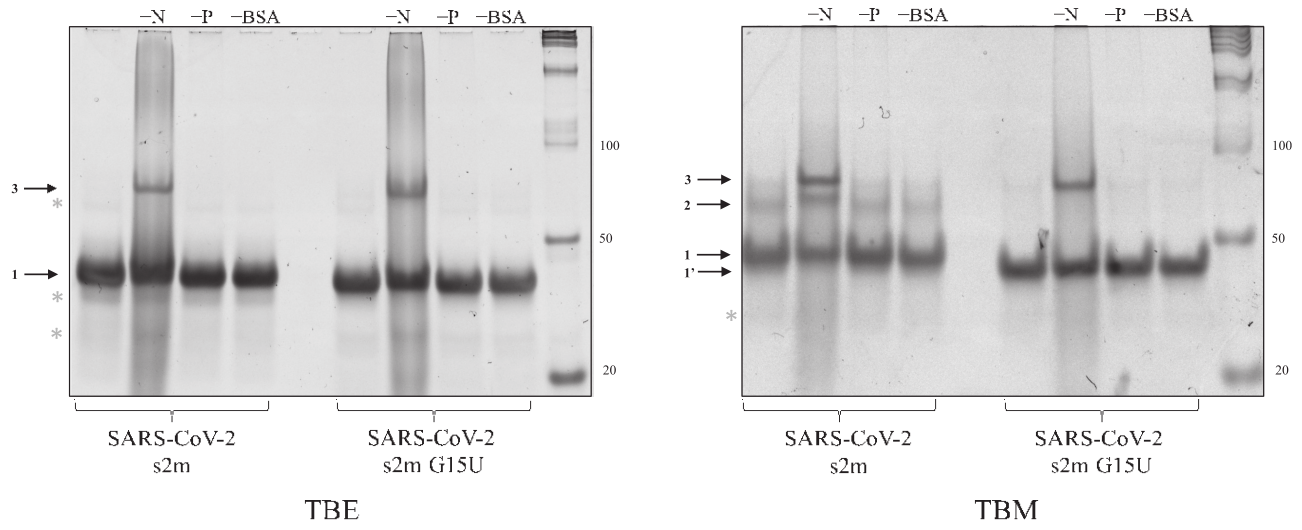

FIGURE 7. Nondenaturing gel electrophoresis of the s2m reference and s2m G15U converted to an ED structure by the viral N protein. Both s2m elements were incubated with 1 µM $MgCl_2$ for 30 min, an additional 30 min with the N protein, and 5 min with proteinase K to digest the proteins prior to the samples being split in TBE (left) and TBM (right) conditions for electrophoresis. In both cases, the s2m remains preferentially monomeric (arrows 1 and 1′). The N protein converted both elements to an ED structure (arrow 3), and in the TBM gel, the N protein also stabilized the KD of the s2m reference (right, arrow 2). However, the band corresponding to the KD of the s2m G15U sample is still not observed. The P protein and BSA were used as controls and had no effect on the conversion of either s2m KD to the duplex conformation.

(Fig. 6 right, arrows 1 and 1′). Moreover, our MD simulation findings show that the monomer s2m G15U is linear, while the original s2m monomer is kinked; this is consistent with this hypothesis (Makowski et al. 2023). Despite these observed differences in the s2m G15U KD versus the s2m reference KD, we further demonstrate that this mutation does not affect the ability of the viral N protein to convert the s2m G15U KD to a stable duplex structure, which is the in vivo process of duplex formation. It has been suggested that the N protein preferentially binds to double-stranded RNA segments in the central region of the s2m, specifically nucleotides G28, G30, and U31, making a stable protein–RNA complex for virion packaging (Padroni et al. 2022; Morse et al. 2023). Therefore, the closing of the U15–A29 base pair, despite making the s2m G15U upper stem more stable, which would be unfavorable for the conversion of the s2m G15U KD to the duplex conformation, may compensate for this unfavorable effect by further assisting in N protein binding.

The findings that the G15U mutation does not affect the ability of the N protein to convert the s2m G15U KD to the duplex conformation are contrasting the effect another single nucleotide mutation in the s2m upper stem (G31U) has on this conversion. In our previous work, we showed that the G31U mutation that exists between the SARS-CoV and SARS-CoV-2 s2m was responsible for drastic differences in the s2m dimerization, even in the presence of the N protein (Imperatore et al. 2022). The SARS-CoV s2m readily forms KDs that could not be converted to the ED by the N protein. Conversely, the SARS-CoV-2 s2m which differs by only 2 nt (only one of which, G31U, we showed is responsible for the dimerization differences) from SARS-CoV s2m, exists primarily as a monomer that forms KDs which are subsequently converted to the duplex conformation by the N protein (Imperatore et al. 2022). While the single nucleotide G31U mutation was shown to be responsible for this difference in s2m dimerization properties between SARS-CoV s2m and the SARS-CoV-2 s2m, we show here that the s2m G15U single nucleotide mutation present in the Delta variant has limited effects on the element's dimerization (Imperatore et al. 2022).

SARS-CoV-2 s2m G15U interactions with miR-1307-3p

We and others previously identified two miR-1307-3p binding sites on the s2m element in the SARS-CoV-2 3′-UTR (Fig. 8A), and we revealed its specificity for this miR (Arisan et al. 2020; Balmeh et al. 2020; Chan et al. 2020; Alam and Lipovich 2021; Imperatore et al. 2022). The exact role of miR-1307-3p in the SARS-CoV-2 infection is not known; however, it has been shown that miR-1307-3p is the highest expressed microRNA in Vero cells infected by SARS-CoV-2, and the levels of miR-1307-3p are elevated in severe cases of COVID-19 as compared with mild cases (Arisan et al. 2022; Zarei Ghobadi et al. 2022). Thus, we investigated if the G15U mutation within the s2m has any effect upon its interactions with miR-1307-3p. The binding interactions between miR-1307-3p and s2m G15U as compared to the s2m reference were assessed by TBE/TBM

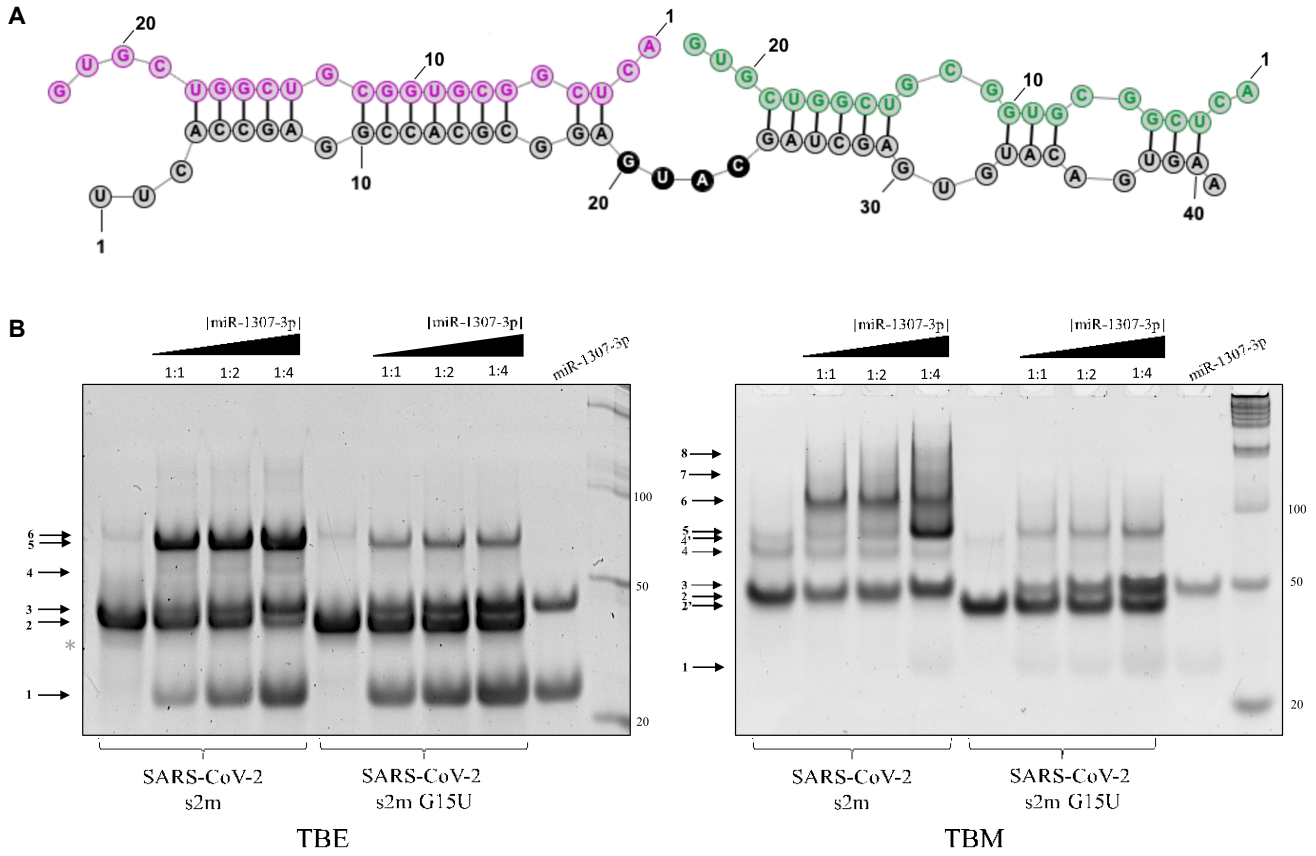

FIGURE 8. (A) Predicted miR-1307-3p binding sites to the s2m. The two miR-1307-3p molecules are shown in purple and green, respectively, whereas s2m is shown in gray. (B) Nondenaturing TBE (left) and TBM (right) gels of s2m and s2m G15U binding to miR-1307-3p in 1:1 and 1:2 and 1:4 s2m:miR ratios in the presence of 1 mM $MgCl_2$. In TBE, both s2m elements prefer their monomeric states (arrow 2), whereas the miR-1307-3p exists as a monomer and dimer (arrows 1 and 3). As miR is added, upper complexes are formed between the two (arrows 4 and 5). Arrow 6 reveals the presence of the ED of the s2ms. Overall, the band intensity of the complexes formed by s2m G15U with miR-1307-3p is re-duced. In TBM conditions, the s2m reference can form a stable complex with two miR-1307-3p (arrow 5) and a complex formed by two s2m each bound to one miR-1307-3p is also apparent (arrow 6). Arrows 7 and 8 indicate higher molecular weight complex that could be potentially formed by RNA LEGO type interactions mediated by the palindromic sequence GUGC at the 3′ end of miR-1307-3p interacting with another miR, as it is bound to a s2m. Arrows 4 and 4′ show the KD and duplex formed by the s2m reference, respectively. The monomers of s2m and s2m G15U mi-grate differently (arrows 2 and 2′), as described in the text.

native PAGE. The s2m and s2m G15U were boiled and snap-cooled, then incubated with 1 mM $MgCl_2$ for 30 min, after which miR-1307-3p was added in 1:1 and 1:2, and 1:4 s2m:miR ratios and incubated for an additional 30 min at 25°C. The samples were then split and electrophoresed in TBE and TBM conditions, respectively. In the TBE gel, two bands are present for miR-1307-3p, a monomer and dimer (Fig. 8B, left, arrows 1 and 3), while both the s2m and s2m G15U are present as monomers (Fig. 8B, left, arrow 2). In the presence of miR-1307-3p, two upper bands become apparent for the s2m, which were assigned to the complex of s2m with one miR-1307-3p molecule (Fig. 8B, left, arrow 4) and two miR-1307-3p molecules, respectively (Fig. 8B, left, arrow 5), given the relative size of the bands compared to the molecular weight marker (Imperatore et al. 2022). However, the intensities of these upper bands are significantly decreased for s2m G15U, suggesting that miR-1307-3p binds less to this mutant. Note that there is a faint band at almost the same position, indicated by arrow 6, in the free s2m and s2m G15U lanes that corresponds to the duplex conformation (82 nt). This is very close in size to the complex formed by s2m with two miR-1307-3p molecules (85 nt), so it can no longer be distinguished as miR is titrated into the sample at higher concentration ratios. When the Mg^{2+} ions are retained in the TBM gel, the complex of the s2m with two miR-1307-3p molecules is stabilized (Fig. 8B, right, arrow 5) and a new higher-order complex appears, which we assigned to an s2m dimer interacting with two miR-1307-3p molecules, as described in our previous work (Fig. 8B, right, arrow 6; Imperatore et al. 2022). Further, arrows 7 and 8, which appear faintly, may be the result of end-to-end RNA LEGO complexes, tertiary RNA assemblies that are Mg^{2+} dependent, mediated by the palindromic sequence CGUG at the 3′ end of

miR-1307-3p, (Fig. 8A; Horiya et al. 2003). In contrast, while Mg^{2+} ions stabilize the complex formed by s2m G15U with two miR-1307-3p molecules (Fig. 8B, right, arrow 5), the band corresponding to the complex formed with s2m G15U is less prominent, and the higher-order complexes seen with the s2m are not apparent. This result suggests that the closing of the U15–A29 base pair creates a more stable s2m upper stem, making it harder for the miR-1307-3p to invade it.

To determine the relative binding affinity difference between the s2m and s2m G15U, a fluorescently tagged miR-1307-3p-DY547 was used in native TBM gels monitoring the fluorescence of DY547 (excitation 558 and emission at 574 nm) (Fig. 9A,B, left), followed by staining in SYBR Gold to observe all RNA bands and overlay with the fluores -cent image (Fig. 9A,B, right). The free miR-1307-3p-DY547, exists as a mixture of monomer and dimer, as monitored by the DY547 fluorescence (Fig. 9A, arrows 1 and 3). However, since the DY547 tag adds bulkiness, miR-1307-3p-DY547 has an altered migration pattern as compared to the unlabeled miR-1307-3p. Three upper bands are observable (Fig. 9, arrows 6, 7, and 8) when increasing ratios of miR-1307-3p-DY547 were incubated with s2m. Similar to the TBM binding gel with the unlabeled miR, we assign the bound complex of one s2m to two miR (arrow 6), a s2m dimer with each s2m bound by one miR (arrow 7), and finally a magnesium-stabilized RNA LEGO interaction complex formed through interactions of the palindromic sequence found at the end of the miR-1307-3p as it is bound to a s2m (arrow 8) (Horiya et al. 2003). To quantify these results, the intensities of the bands corresponding to the miR-1307-3p-DY547 complexes with s2m (arrows 6, 7, and 8) were measured using the ImageJ gel analysis software (Gallagher 2010) and normalized to the relative intensity of the free miR-1307-3p-DY547 lane (arrows 1 and 3). These experiments were performed in triplicate, and the averaged, normalized relative band intensities were in the range of 0.19–1.32 for the miR:s2m ratios of 0.25–4 miR (Fig. 9A, left, bottom of the gel and Fig. 9C). In the s2m G15U gel, like in the TBM binding gel with the unlabeled miR, only the complex formed by one s2m G15U with two copies of miR-1307-3p-DY547 is observed (Fig. 9B, arrow 5). After normalizing the intensity of the band corresponding to the miR-1307-3p-DY547 complex with s2m G15U (arrow 5) to that of the free miR-1307-3p-DY547 (arrows 1 and 3), the average, normalized relative band intensity across the triplicate experiments was in the range of 0.07–0.48 for the miR:s2m G15U ratios of 0.25–4 miR (Fig. 9B, left, bottom of the gel and Fig. 9C). Taken together these results indicate that miR-1307-3p-DY547 has reduced binding to s2m G15U, as compared to the s2m reference (Fig. 9C).

Disease severity in patients with SARS-CoV-2 has fluctuated throughout the pandemic, ranging from asymptomatic to mild to severe. In severe cases of COVID-19, hyperactive immune responses lead to the overproduction and release of cytokines, termed the "cytokine storm." These cytokines are proteins critical for the regulation of the host's defense mechanisms (Vial and Descotes 1995). An example of cytokines includes interleukins (ILs), such as IL18, and their receptors (e.g., IL6R, IL10RA, IL10RB, IL12RB2, IL17RA), and it has been shown that their overexpression is linked to the onset of cytokine storms in COVID-19 patients (Agarwal et al. 2015). A suggested regulator of these ILs and their receptors is host miR-1307-3p (Mehta et al. 2020; Yang et al. 2020; Imperatore et al. 2022). MiR-1307-3p has also been proposed to reduce glucose regulating protein 78 (GRP78), a protein thought to aid in binding of the SARS-CoV-2 S protein to the host cell's receptors (Elfiky 2020; Ibrahim et al. 2020; Carlos et al. 2021). By allowing the virus to hijack this miR, GRP78 abundance in the cells would be increased, aiding viral entry into the cell. Viruses have been shown to hijack host miRNAs for their own benefit (Guo and Steitz 2014; Trobaugh and Klimstra 2017). One example of this is HCV, which uses miR-122 to enhance its replication (Jopling et al. 2005; Shimakami et al. 2012). Previously, upon finding that the s2m binds two copies of miR-1307-3p, we proposed that this miR is hijacked by SARS-CoV-2 for the benefit of the virus (Imperatore et al. 2022). However, considering these new results, our previous hypothesis must be amended as it seems that the virus has evolved to reduce its interactions with this miR in the Delta variant. We show that the s2m G15U binds to less miR-1307-3p as compared to the s2m reference and suggest the newly formed U15–A29 base pair formation as causative for these diminished interactions, as the s2m upper stem must be opened for new base pairs to be formed with miR-1307-3p. This implies that miR-1307-3p may instead have a detrimental effect on the virus, as our data supports that the virus preferentially evolved to reduce this interaction. Recent work has identified that host miRs may target the viral genome as part of the immune response, in which case, the virus would preferentially evolve to evade this attack (Lecellier et al. 2005; Huang et al. 2007; Otsuka et al. 2007; Skalsky and Cullen 2010). MiRs normally bind to the target mRNA 3′-UTR to signal its degradation and/or to regulate its translation (O'Brien et al. 2018). Often, the miR binding sites on mammalian mRNAs are highly conserved, preserving the regulatory role of these miRs (Friedman et al. 2009). Given the high conservation of the s2m in the 3′-UTR of several viral families, it is possible that the host immune response could use miRs to target this element, and several miRs are dysregulated upon SARS-CoV-2 infection (Farr et al. 2021). Thus, by targeting the s2m of SARS-CoV-2, the host may be utilizing miR-1307-3p to alter the translation of viral proteins (Panda et al. 2022). It is interesting to note that since the SARS-CoV-2 subgenomic RNAs share the same 3′-UTR with the genomic RNA, miR-1307-3p could target the translation of both the viral structural and nonstructural

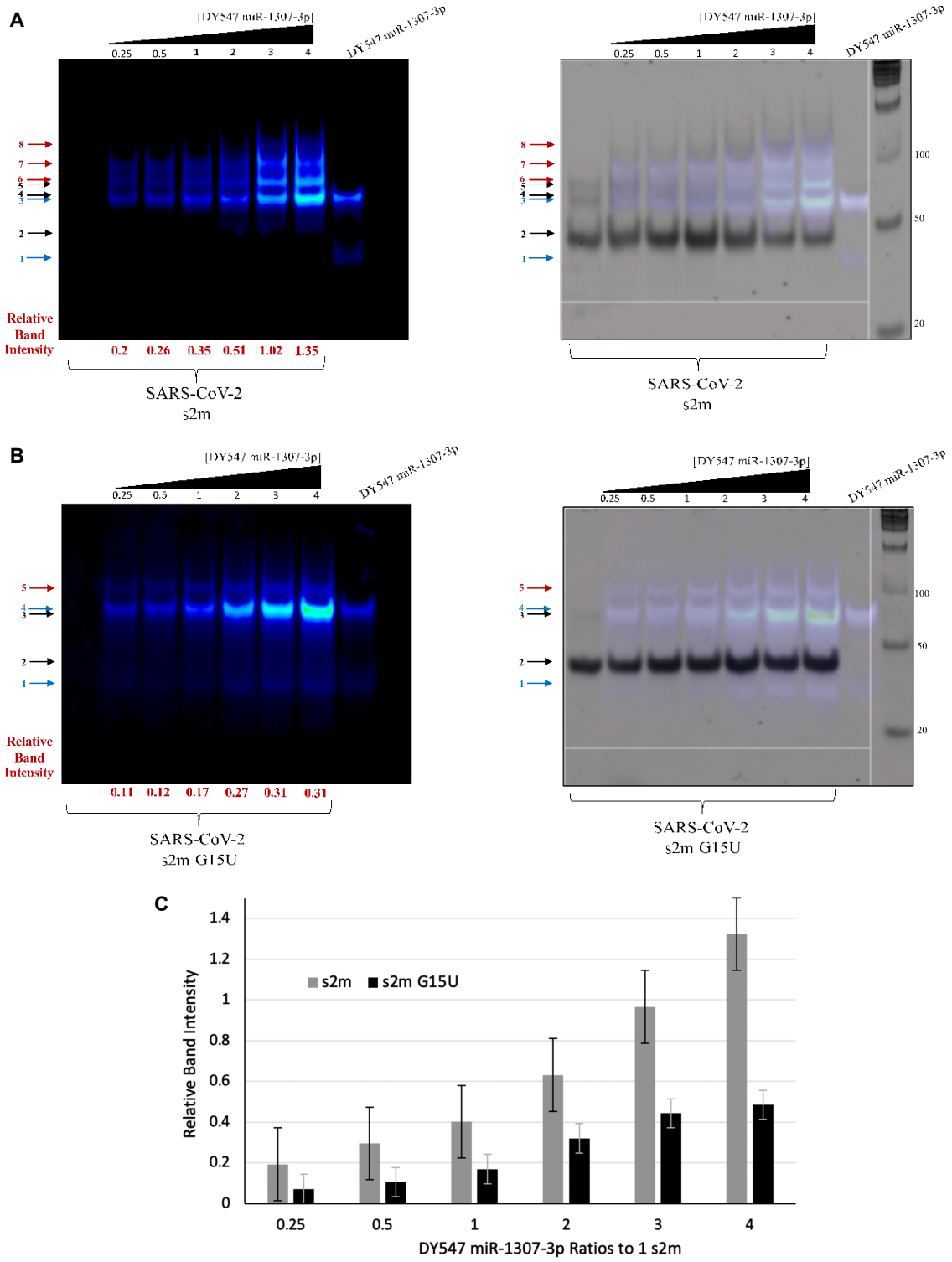

FIGURE 9. Nondenaturing TBM gel of s2m and s2m G15U binding to a fluorescently tagged DY547 miR-1307-3p in ratios ranging from 1:0.25 to 1:4 s2m:miR in the presence of 1 mM $MgCl_2$. The gels were visualized with a fluorescent imager at 600 nm wavelength (left), stained with SYBR Gold, then overlaid (right). (A) In the s2m binding gels, the blue arrows 1 and 3 correspond to the free DY547 miR-1307-3p in its monomeric and dimeric state, respectively. Arrow 2 indicates the monomeric s2m, whereas arrows 4 and 5 represent the KD and ED, respectively. Bound complex arrows that were used for quantification are indicated in red and show the s2m bound to two miR (arrow 6), the s2m dimer bound to two miRs (one miR to one s2m) (arrow 7), and complexes formed by end-to-end palindromic sequence interactions of the miR bound to the s2m (arrow 8). (B) When the miR is bound to the s2m G15U in TBM conditions, the miR exists as both a monomer and dimer, arrows 1 and 4, respectively. Arrow 2 indicates the monomeric s2m G15U, whereas arrow 3 represents a dimeric form, and these are only present in the right image of the gel stained in SYBR Gold due to it lacking a fluorescent tag. A bound complex between the s2m and two DY547 miR-1307-3p is indicated by arrow 5. Relative band intensities of the bound complexes (red arrows) were calculated using ImageJ as described in the text, and the intensities of the shown gels are listed. (C) The relative band intensities were averaged across the triplicate experiments (representative images shown in A and B). Across all miR ratios, the s2m consistently had a higher relative band intensity of its complexes than the s2m G15U. The standard deviation is included.

proteins. The host miR-1307-3p has been shown to be upregulated in SARS-CoV-2 infected cells, up to a 38-fold increase, and is implicated in the silencing of SARS-CoV-2 post-transcriptionally (Arisan et al. 2022; Panda et al. 2022; Zarei Ghobadi et al. 2022). Additionally, increased expression of miR-1307-3p has been shown to result in decreased replication of the SARS-CoV-2 genome (Soremekun et al. 2020; Zarei Ghobadi et al. 2022). Therefore, mutations which decrease the binding interactions of miR-1307-3p with the s2m, such as those we observe in the s2m G15U mutant, would be optimal for overall viral fitness of Delta compared to the previous variants that contain the s2m.

Interestingly, our recent work has shown that the Omicron variant, the most prominent viral strain to emerge after Delta, contains a 26 nt deletion within the s2m element that eliminates the miR-1307-3p binding sites (Colson et al. 2022; Frye et al. 2023). Omicron has also been shown to have further reduced disease severity and increased infectivity when compared to Delta and other prior variants (Chaguza et al. 2022). We emphasize that our results could be evidence of a stepwise reduction of the miR-1307-3p binding sites as the s2m has evolved to reduce miR-1307-3p binding in Delta and subsequently removed the binding sites with the 26 nt deletion in Omicron (Frye et al. 2023). This trend supports the notion that SARS-CoV-2 is evolving toward reduced miR-1307-3p binding. Despite the lack of knowledge regarding this interaction, we suspect that if miR-1307-3p is in fact a crucial player in the antiviral immune response, the Omicron variant of SARS-CoV-2 greatly benefits through an overall reduced miR-1307-3p binding. Further, if miR-1307-3p is involved in the "cytokine storm," this variant also benefits through lower disease severity, which is seen in patients diagnosed with the Omicron variant. Sequence alignments of the SARS-CoV-2 variants to other coronaviruses, specifically human "cold-like" viruses, revealed that the Omicron deletion within the s2m is similar to those of the common cold (Arisan et al. 2022). This further supports that the removal of this region, and the decreased (or lack of) ability to bind miR-1307-3p may be a similar evolutionary step taken by SARS-CoV-2 to prevent severe, and potentially deadly, symptoms in the host by improving its evasion of the host immune response.

However, it is to be acknowledged that this data alone cannot prove directly if this s2m G15U mutant does indeed confer a selective advantage to SARS-CoV-2, or is a result of a hitchhiking effect, where the mutations within the S protein, which conferred an advantage to the Delta variant, happened on a genome that already had the s2m G15U mutation. Nonetheless, the findings that the Omicron variant, which is not a direct descendant of the Delta variant, acquired the 26 nt deletion that removed the miR-1307-3p binding sites suggest that the abolishment of the miR-1307-3p interactions with the genomic and subgenomic viral RNA is advantageous to the virus. Further research is needed to elucidate the details of the role of miR-1307-3p in the host immune response to SARS-CoV-2 infections and viral genome dimerization.

In summary, we showed here that the s2m G15U mutation is present in 99.32% of the SARS-CoV-2 Delta variant, and that while this mutation does not affect the s2m dimerization properties in the presence of the N protein, it does reduce its ability to interact with host miR-1307-3p, potentially having implications on the host response to SARS-CoV-2 infection and viral evolution to evade this response.

MATERIALS AND METHODS

Bioinformatics analysis

SARS-CoV-2 genomes were retrieved from the Global Initiative on Sharing All Influenza Data (GISAID) EpiCoV platform for the period of April 2020 to October 2021, and to facilitate alignment, only complete and high-coverage genomes were selected. The hCoV-19 Wuhan SARS-CoV-2 virus (GISAID: EPI_ISL_402123) was used as a reference genome (Wu et al. 2020). Analysis of the s2m was performed using a custom R script dependent on the packages BiocManager, Biostrings, DECIPHER, hiReadsProcessor, adegenet, stringr, and ape, which was recently used to monitor s2m sequence and identify mutations (Huber et al. 2015; Frye et al. 2023). To manipulate and align sequences, we used the Biostrings and DECIPHER packages, managed by BiocManager. We trimmed aligned sequences to the s2m with a hiReadsProcessor and used adegenet, stringr, and ape for further processing and identification of mutations within s2m. The SARS-CoV-2 reference sequence was converted to a FASTA file and added to each batch of sequences, which contained less than 10,000 sequences each. The first 29,000 nt of each sequence were removed to reduce computational time, and the sequences were realigned at the 3′ end. After performing the alignment, the script identified sequences with single nucleotide insertions that disrupt mutation identification by introducing gaps in all other sequences in the alignment. These sequences were removed, and the remaining sequences were realigned. From a total of 2,034,376 sequences analyzed, 1980 were found to have single nucleotide insertions and were removed from this analysis. The script then extracted the s2m motif from all sequences in the final alignment and identified mutations relative to the reference sequence. Mutations and corresponding information, including accession ID, geographic location, and collection date, were output in a CSV file. The sequence alignments were completed for each of the SARS-CoV-2 variants and each geographical location of interest. These data were then processed and used for the identification of s2m mutation trends. This was repeated for India, where we input data sets of either Delta (23,733 sequences) or Kappa (2982 sequences) variants and determined the s2m G15U percentage for each variant. For both Delta and Kappa, no sequences were removed due to insertions. As a control, we repeated the bioinformatics analysis for the Alpha variant (937,040 sequences) and found 102,453 sequences to be removed (10.93%), then analyzed Alpha for s2m mutations.

TABLE 1. Oligonucleotide sequences used in this study

SARS-CoV-2 s2m	5′ UUCACCGAGGCCACGCGGAGUACGAUCGAGUGUACAGUGAA 3′
SARS-CoV-2 s2m G15U	5′ UUCACCGAGGCCACUCGGAGUACGAUCGAGUGUACAGUGAA 3′
miR-1307-3p	5′ ACUCGGCGUGGCGUCGGUCGUG 3′
miR-1307-3p-DY547	5′ ACUCGGCGUGGCGUCGGUCGUG-DY547 3′

RNA samples

The s2m and miR RNA sequences used in this study (Table 1) were purchased from Dharmacon Inc. and resuspended in 10 mM cacodylic acid, pH 6.5.

Nondenaturing polyacrylamide gel electrophoresis

The RNA samples were diluted in ½× Tris-Boric Acid (TB) buffer to 1 µM, boiled for 5 min, then snap-cooled in dry ice and ethanol, after which the samples were incubated at 25°C for 1 h in the presence of varying concentrations between 1 mM and 10 mM of $MgCl_2$. To evaluate the conversion of the KD to a thermodynamically stable ED, 1 µM s2m and s2m G15U RNAs were incubated with 1 mM $MgCl_2$ for 30 min, followed by an additional 30-min incubation with 2 µM N protein (RayBiotech Inc., catalog #230-01104). The SARS-CoV-2 main protease (P) protein (R&D Systems, catalog #E-720-050) and BSA (Thermo Fisher, catalog #15561020) were used as control proteins. Prior to electrophoresing, proteinase K (New England Biolabs) was added for 10 min to digest the proteins. To analyze the interactions between the s2m and s2m G15U and miR-1307-3p, 1 µM s2m RNA was incubated with 1 mM $MgCl_2$ for 30 min, followed by an additional incubation with increasing concentration ratios of miR-1307-3p for 30 min. For all experiments, a glycerol-based loading buffer was added to increase the sample density, then they were evenly split after incubation and run in two separate gel conditions: nondenaturing 12% Tris-Boric Acid EDTA (TBE) or 12% Tris-Boric Acid with 5 mM $MgCl_2$ (TBM), made with 30:08 acrylamide:bis-acrylamide. The samples were electrophoresed for 2 h at 75 V in TBE and 4 h in TBM using ½× TBE and ½× TBM running buffer, respectively. Visualization of the gels was done by staining in SYBR Gold cyanide dye and UV transillumination at 537 nm on an AlphaImager. All experiments were completed in triplicate.

To quantify binding interactions between the s2m or s2m G15U to the miR, we used a fluorescently tagged DY547 miR-1307-3p. These experiments were conducted similarly; 1 µM s2m RNA was incubated with 1 mM $MgCl_2$ for 30 min followed by incubation with increasing concentration ratios of miR-1307-3p-DY547 for 30 min. The samples were electrophoresed for 4 h at 75 V on a TBM nondenaturing gel. To visualize the bound complexes, the gel was visualized using a LI-COR Odyssey Fc on the 600 nm channel, then stained in SYBR Gold cyanide dye and visualized using UV transillumination at 537 nm on an AlphaImager to overlay the images and confer the band identities. The relative band intensities of the fluorescent bound complexes were calculated using the ImageJ gel analysis software (Gallagher 2010). The calculations were normalized to the total intensity of the free DY547 miR-1307-3p (1 µM). These experiments were completed in triplicate, and the relative intensity from each was averaged and then used to calculate the standard deviation.

^{1}H NMR spectroscopy

One-dimensional ^{1}H NMR spectroscopy of the s2m reference and s2m G15U was performed at 19°C on a 500 MHz Bruker AVANCE NMR spectrometer equipped with TopSpin 3.2 acquisition software. RNA samples at a concentration of 220 µM were prepared in 10 mM cacodylic acid, pH 6.5, in a 90:10 H_2O:D_2O ratio. Samples were boiled for 5 min and snap-cooled using dry ice and ethanol prior to data acquisition. Water suppression was carried out using the Watergate pulse sequence (Piotto et al. 1992).

A ^{1}H–^{1}H NOESY experiment with a 150 msec mixing time was conducted for s2m G15U at 19°C on a 500 MHz Bruker AVANCE spectrometer. The sample was prepared at 250 µM RNA in 10 mM cacodylic acid buffer, pH 6.5, in a 90% H_2O:10% D_2O ratio.

UV thermal denaturation

UV thermal denaturation data curves were collected using a Varian Cary E3 UV–visible spectrophotometer attached to a Peltier temperature control. Each RNA sample was 10 µM in 10 mM cacodylic acid, pH 6.5, and had a layer of mineral oil on top to prevent evaporation. The samples were heated at a rate of 0.2°C/min from 25°C to 95°C with a 3 min hold. The absorbance was recorded at 260 nm, a wavelength sensitive to hairpin dissociation (Draper and Gluick 1995; Davis et al. 1998). The data were normalized, and the first derivative processed with exponential smoothing was used to determine the melting temperature, T_m, of each sample.

SUPPLEMENTAL MATERIAL

Supplemental material is available for this article.

ACKNOWLEDGMENTS

This research was supported by National Science Foundation (NSF) CHE-2029124 RAPID (M.-R.M., J.D.E.), NSF MRI Supercomputer CHE-1726824, NSF CHE-2244151 REU (P.E.L., J.D.E.), and National Institutes of Health (NIH) 2R15GM127307-05 (M.-R.M.) grants.

Received February 10, 2023; accepted July 30, 2023.

REFERENCES

Aagaard L, Rasmussen SV, Mikkelsen JG, Pedersen FS. 2004. Efficient replication of full-length murine leukemia viruses modified at the dimer initiation site regions. Virology 318: 360–370. doi:10.1016/j.virol.2003.09.008

Aduri R, Briggs KT, Gorelick RJ, Marino JP. 2013. Molecular determinants of HIV-1 NCp7 chaperone activity in maturation of the HIV-1 dimerization initiation site. Nucleic Acids Res 41: 2565–2580. doi:10.1093/nar/gks1350

Agarwal V, Bell GW, Nam J-W, Bartel DP. 2015. Predicting effective microRNA target sites in mammalian mRNAs. Elife 4: e05005. doi:10.7554/eLife.05005

Alam T, Lipovich L. 2021. miRCOVID-19: potential targets of human miRNAs in SARS-CoV-2 for RNA-based drug discovery. Noncoding RNA 7: 18. doi:10.3390/ncrna7010018

Andersen ES, Jeeninga RE, Damgaard CK, Berkhout B, Kjems J. 2003. Dimerization and template switching in the 5′ untranslated region between various subtypes of human immunodeficiency virus type 1. J Virol 77: 3020–3030. doi:10.1128/JVI.77.5.3020-3030.2003

Andrews N, Stowe J, Kirsebom F, Toffa S, Rickeard T, Gallagher E, Gower C, Kall M, Groves N, O'Connell A-M, et al. 2022. Covid-19 vaccine effectiveness against the Omicron (B.1.1.529) variant. N Engl J Med 386: 1532–1546. doi:10.1056/NEJMoa2119451

Arisan ED, Dart A, Grant GH, Arisan S, Cuhadaroglu S, Lange S, Uysal-Onganer P. 2020. The prediction of miRNAs in SARS-CoV-2 genomes: hsa-miR databases identify 7 Key miRs linked to host responses and virus pathogenicity-related KEGG pathways significant for comorbidities. Viruses 12: 614. doi:10.3390/v12060614

Arisan ED, Dart DA, Grant GH, Dalby A, Kancagi DD, Turan RD, Yurtsever B, Karakus GS, Ovali E, Lange S, et al. 2022. microRNA 1307 is a potential target for SARS-CoV-2 infection: an in vitro model. ACS Omega 7: 38003–38014. doi:10.1021/acsomega.2c05245

Balmeh N, Mahmoudi S, Mohammadi N, Karabedianhajiabadi A. 2020. Predicted therapeutic targets for COVID-19 disease by inhibiting SARS-CoV-2 and its related receptors. Inform Med Unlocked 20: 100407. doi:10.1016/j.imu.2020.100407

Berkhout B, van Wamel JL. 1996. Role of the DIS hairpin in replication of human immunodeficiency virus type 1. J Virol 70: 6723–6732. doi:10.1128/jvi.70.10.6723-6732.1996

Berkhout B, Ooms M, Beerens N, Huthoff H, Southern E, Verhoef K. 2002. In vitro evidence that the untranslated leader of the HIV-1 genome is an RNA checkpoint that regulates multiple functions through conformational changes. J Biol Chem 277: 19967–19975. doi:10.1074/jbc.M200950200

Carabelli AM, Peacock TP, Thorne LG, Harvey WT, Hughes J, de Silva TI, Peacock SJ, Barclay WS, de Silva TI, Towers GJ, et al. 2023. SARS-CoV-2 variant biology: immune escape, transmission and fitness. Nat Rev Microbiol 21: 162–177. doi:10.1038/s41579-022-00841-7

Carlos AJ, Ha DP, Yeh D-W, Krieken RV, Tseng C-C, Zhang P, Gill P, Machida K, Lee AS. 2021. The chaperone GRP78 is a host auxiliary factor for SARS-CoV-2 and GRP78 depleting antibody blocks viral entry and infection. J Biol Chem 296: 100759. doi:10.1016/j.jbc.2021.100759

Caserta LC, Martins M, Butt SL, Hollingshead NA, Covaleda LM, Ahmed S, Everts MRR, Schuler KL, Diel DG. 2023. White-tailed deer (Odocoileus virginianus) may serve as a wildlife reservoir for nearly extinct SARS-CoV-2 variants of concern. Proc Natl Acad Sci 120: e2215067120. doi:10.1073/pnas.2215067120

CDC. 2020a. Coronavirus disease 2019 (COVID-19). Centers for Disease Control and Prevention. https://www.cdc.gov/coronavirus/2019-ncov/variants/variant-classifications.html

CDC. 2020b. COVID data tracker. Centers for Disease Control and Prevention. https://covid.cdc.gov/covid-data-tracker

CDC. 2022. Omicron variant: what you need to know. Centers for Disease Control and Prevention. https://www.cdc.gov/coronavirus/2019-ncov/variants/omicron-variant.html

Chaguza C, Coppi A, Earnest R, Ferguson D, Kerantzas N, Warner F, Young HP, Breban MI, Billig K, Koch RT, et al. 2022. Rapid emergence of SARS-CoV-2 Omicron variant is associated with an infection advantage over Delta in vaccinated persons. Med (NY) 3: 325–334.e4. doi:10.1016/j.medj.2022.03.010

Chan AP, Choi Y, Schork NJ. 2020. Conserved genomic terminals of SARS-CoV-
2 as coevolving functional elements and potential therapeutic targets. mSphere 5: e00754-20. doi:10.1128/mSphere.00754-20

Colson P, Delerce J, Marion-Paris E, Lagier J-C, Levasseur A, Fournier P-E, Scola BL, Raoult D. 2022. A 21L/BA.2-21K/BA.1 "MixOmicron" SARS-CoV-2 hybrid undetected by qPCR that screen for variant in routine diagnosis. Infect Genet Evol 105: 105360. doi:10.1016/j.meegid.2022.105360

Davis TM, McFail-Isom L, Keane E, Williams LD. 1998. Melting of a DNA hairpin without hyperchromism. Biochemistry 37: 6975–6978. doi:10.1021/bi980047l

Draper DE, Gluick TC. 1995. Melting studies of RNA unfolding and RNA–ligand interactions. Methods Enzymol 259: 281–305. doi:10.1016/0076-6879(95)59049-8

Dubois N, Marquet R, Paillart J-C, Bernacchi S. 2018. Retroviral RNA dimerization: from structure to functions. Front Microbiol 9: 527. doi:10.3389/fmicb.2018.00527

Duong D. 2021. Alpha, Beta, Delta, Gamma: What's important to know about SARS-CoV-2 variants of concern? CMAJ 193: E1059–E1060. doi:10.1503/cmaj.1095949

Elbe S, Buckland-Merrett G. 2017. Data, disease and diplomacy: GISAID's innovative contribution to global health: data, disease and diplomacy. Glob Chall 1: 33–46. doi:10.1002/gch2.1018

Elfiky AA. 2020. SARS-CoV-2 spike-heat shock protein A5 (GRP78) recognition may be related to the immersed human coronaviruses. Front Pharmacol 11: 577467. doi:10.3389/fphar.2020.577467

Ennifar E, Yusupov M, Walter P, Marquet R, Ehresmann B, Ehresmann C, Dumas P. 1999. The crystal structure of the dimerization initiation site of genomic HIV-1 RNA reveals an extended duplex with two adenine bulges. Structure 7: 1439–1449. doi:10.1016/S0969-2126(00)80033-7

Farinholt T, Doddapaneni H, Qin X, Menon V, Meng Q, Metcalf G, Chao H, Gingras M-C, Avadhanula V, Farinholt P, et al. 2021. Transmission event of SARS-CoV-2 Delta variant reveals multiple vaccine breakthrough infections. BMC Med 19: 255. doi:10.1186/s12916-021-02103-4

Farr RJ, Rootes CL, Rowntree LC, Nguyen THO, Hensen L, Kedzierski L, Cheng AC, Kedzierska K, Au GG, Marsh GA, et al. 2021. Altered microRNA expression in COVID-19 patients enables identification of SARS-CoV-2 infection. PLoS Pathog 17: e1009759. doi:10.1371/journal.ppat.1009759

Friedman RC, Farh KK-H, Burge CB, Bartel DP. 2009. Most mammalian mRNAs are conserved targets of microRNAs. Genome Res 19: 92–105. doi:10.1101/gr.082701.108

Frye CJ, Shine M, Makowski JA, Kensinger AH, Cunningham CL, Milback EJ, Evanseck JD, Lackey PE, Mihailescu MR. 2023. Bioinformatics analysis of the s2m mutations within the SARS-CoV-2 Omicron lineages. J Med Virol 95: e28141. doi:10.1002/jmv.28141

Gallagher SR. 2010. Digital image processing and analysis with ImageJ. Curr Protoc 3: A.3C.1–A.3C.24. doi:10.1002/9780470089941.eta03cs9

Gilbert C, Tengs T. 2021. No species-level losses of s2m suggests critical role in replication of SARS-related coronaviruses. Sci Rep 11: 16145. doi:10.1038/s41598-021-95496-4

Greatorex J. 2004. The retroviral RNA dimer linkage: different structures may reflect different roles. Retrovirology 1: 22. doi:10.1186/1742-4690-1-22

Guo YE, Steitz JA. 2014. Virus meets host microRNA: the destroyer, the booster, the hijacker. Mol Cell Biol 34: 3780–3787. doi:10.1128/MCB.00871-14

Horiya S, Li X, Kawai G, Saito R, Katoh A, Kobayashi K, Harada K. 2003. RNA LEGO: magnesium-dependent formation of specific RNA assemblies through kissing interactions. Chem Biol 10: 645–654. doi:10.1016/S1074-5521(03)00146-7

Huang J, Wang F, Argyris E, Chen K, Liang Z, Tian H, Huang W, Squires K, Verlinghieri G, Zhang H. 2007. Cellular microRNAs contribute to HIV-1 latency in resting primary $CD4^+$ T lymphocytes. Nat Med 13: 1241–1247. doi:10.1038/nm1639

Huber W, Carey VJ, Gentleman R, Anders S, Carlson M, Carvalho BS, Bravo HC, Davis S, Gatto L, Girke T, et al. 2015. Orchestrating high-throughput genomic analysis with Bioconductor. Nat Methods 12: 115–121. doi:10.1038/nmeth.3252

Ibrahim IM, Abdelmalek DH, Elshahat ME, Elfiky AA. 2020. COVID-19 spike-host cell receptor GRP78 binding site prediction. J Infect 80: 554–562. doi:10.1016/j.jinf.2020.02.026

Imperatore JA, Cunningham CL, Pellegrene KA, Brinson RG, Marino JP, Evanseck JD, Mihailescu MR. 2022. Highly conserved s2m element of SARS-CoV-2 dimerizes via a kissing complex and interacts with host miRNA-1307-3p. Nucleic Acids Res 50: 1017–1032. doi:10.1093/nar/gkab1226

Jonassen CM. 2008. Detection and sequence characterization of the 3′-end of coronavirus genomes harboring the highly conserved RNA motif s2m. Methods Mol Biol 454: 27–34. doi:10.1007/978-1-59745-181-9_3

Jopling CL, Yi M, Lancaster AM, Lemon SM, Sarnow P. 2005. Modulation of hepatitis C virus RNA abundance by a liver-specific MicroRNA. Science 309: 1577–1581. doi:10.1126/science.1113329

Jung C, Kmiec D, Koepke L, Zech F, Jacob T, Sparrer KMJ, Kirchhoff F. 2022. Omicron: what makes the latest SARS-CoV-2 variant of concern so concerning? J Virol 96: e02077-21. doi:10.1128/jvi.02077-21

Kannan SR, Spratt AN, Cohen AR, Naqvi SH, Chand HS, Quinn TP, Lorson CL, Byrareddy SN, Singh K. 2021. Evolutionary analysis of the Delta and Delta Plus variants of the SARS-CoV-2 viruses. J Autoimmun 124: 102715. doi:10.1016/j.jaut.2021.102715

Kensinger AH, Makowski JA, Pellegrene KA, Imperatore JA, Cunningham CL, Frye CJ, Lackey PE, Mihailescu MR, Evanseck JD. 2022. Structural, dynamical, and entropic differences between SARS-CoV and SARS-CoV-2 s2m elements using molecular dynamics simulations. ACS Phys Chem Au 3: 30–43. doi:10.1021/acsphyschemau.2c00032

Kenyon JC, Prestwood LJ, Le Grice SFJ, Lever AML. 2013. In-gel probing of individual RNA conformers within a mixed population reveals a dimerization structural switch in the HIV-1 leader. Nucleic Acids Res 41: e174. doi:10.1093/nar/gkt690

Lecellier C-H, Dunoyer P, Arar K, Lehmann-Che J, Eyquem S, Himber C, Saïb A, Voinnet O. 2005. A cellular microRNA mediates antiviral defense in human cells. Science 308: 557–560. doi:10.1126/science.1108784

Li X, Horiya S, Harada K. 2006. An efficient thermally induced RNA conformational switch as a framework for the functionalization of RNA nanostructures. J Am Chem Soc 128: 4035–4040. doi:10.1021/ja0572093

Liu Y, Rocklöv J. 2021. The reproductive number of the Delta variant of SARS-CoV-2 is far higher compared to the ancestral SARS-CoV-2 virus. J Travel Med 28: taab124. doi:10.1093/jtm/taab124

Liu Y, Liu J, Johnson BA, Xia H, Ku Z, Schindewolf C, Widen SG, An Z, Weaver SC, Menachery VD, et al. 2022. Delta spike P681R mutation enhances SARS-CoV-2 fitness over Alpha variant. Cell Rep 39: 110829. doi:10.1016/j.celrep.2022.110829

Lulla V, Wandel MP, Bandyra KJ, Ulferts R, Wu M, Dendooven T, Yang X, Doyle N, Oerum S, Beale R, et al. 2021. Targeting the conserved stem loop 2 motif in the SARS-CoV-2 genome. J Virol 95: e00663-21. doi:10.1128/JVI.00663-21

Luo CH, Morris CP, Sachithanandham J, Amadi A, Gaston D, Li M, Swanson NJ, Schwartz M, Klein EY, Pekosz A, et al. 2021. Infection with the SARS-CoV-2 Delta variant is associated with higher infectious virus loads compared to the Alpha variant in both unvaccinated and vaccinated individuals. Clin Infect Dis 75: e715–e725. doi:10.1093/cid/ciab986

Makowski JA, Kensinger AH, Cunningham CL, Frye CJ, Shine M, Lackey PE, Mihailescu MR, Evanseck JD. 2023. Delta SARS-CoV-2 s2m structure, dynamics, and entropy: consequences of the G15U mutation. ACS Phys Chem Au doi:10.1021/acsphyschemau.3c00008

Malone B, Urakova N, Snijder EJ, Campbell EA. 2022. Structures and functions of coronavirus replication–transcription complexes and their relevance for SARS-CoV-2 drug design. Nat Rev Mol Cell Biol 23: 21–39. doi:10.1038/s41580-021-00432-z

Markov PV, Ghafari M, Beer M, Lythgoe K, Simmonds P, Stilianakis NI, Katzourakis A. 2023. The evolution of SARS-CoV-2. Nat Rev Microbiol 21: 361–379. doi:10.1038/s41579-023-00878-2

Masante C, Jaubert C, Palau W, Plissonneau J, Besnard L, Ventura M, Di Primo C. 2015. Mutations of the SL2 dimerization sequence of the hepatitis C genome abrogate viral replication. Cell Mol Life Sci 72: 3375–3385. doi:10.1007/s00018-015-1893-3

Mehta P, McAuley DF, Brown M, Sanchez E, Tattersall RS, Manson JJ, HLH Across Speciality Collaboration UK. 2020. COVID-19: consider cytokine storm syndromes and immunosuppression. Lancet 395: 1033–1034. doi:10.1016/S0140-6736(20)30628-0

Meng B, Abdullahi A, Ferreira IATM, Goonawardane N, Saito A, Kimura I, Yamasoba D, Gerber PP, Fatihi S, Rathore S, et al. 2022. Altered TMPRSS2 usage by SARS-CoV-2 Omicron impacts infectivity and fusogenicity. Nature 603: 706–714. doi:10.1038/s41586-022-04474-x

Mihailescu M-R, Marino JP. 2004. A proton-coupled dynamic conformational switch in the HIV-1 dimerization initiation site kissing complex. Proc Natl Acad Sci 101: 1189–1194. doi:10.1073/pnas.0307966100

Mikkelsen JG, Lund AH, Duch M, Pedersen FS. 2000. Mutations of the kissing-loop dimerization sequence influence the site specificity of murine leukemia virus recombination in vivo. J Virol 74: 600–610. doi:10.1128/JVI.74.2.600-610.2000

Moore MD, Nikolaitchik OA, Chen J, Hammarskjöld M-L, Rekosh D, Hu W-S. 2009. Probing the HIV-1 genomic RNA trafficking pathway and dimerization by genetic recombination and single virion analyses. PLoS Pathog 5: e1000627. doi:10.1371/journal.ppat.1000627

Morris A, Marsden M, Halcrow K, Hughes ES, Brettle RP, Bell JE, Simmonds P. 1999. Mosaic structure of the human immunodeficiency virus type 1 genome infecting lymphoid cells and the brain: evidence for frequent in vivo recombination events in the evolution of regional populations. J Virol 73: 8720–8731. doi:10.1128/JVI.73.10.8720-8731.1999

Morse M, Sefcikova J, Rouzina I, Beuning PJ, Williams MC. 2023. Structural domains of SARS-CoV-2 nucleocapsid protein coordinate to compact long nucleic acid substrates. Nucleic Acids Res 51: 290–303. doi:10.1093/nar/gkac1179

Muriaux D, De Rocquigny H, Roques BP, Paoletti J. 1996. NCp7 activates HIV-1_{Lai} RNA dimerization by converting a transient loop-loop complex into a stable dimer. J Biol Chem 271: 33686–33692. doi:10.1074/jbc.271.52.33686

O'Brien J, Hayder H, Zayed Y, Peng C. 2018. Overview of microRNA biogenesis, mechanisms of actions, and circulation. Front Endocrinol 9: 402. doi:10.3389/fendo.2018.00402

Otsuka M, Jing Q, Georgel P, New L, Chen J, Mols J, Kang YJ, Jiang Z, Du X, Cook R, et al. 2007. Hypersusceptibility to vesicular stomatitis virus infection in Dicer1-deficient mice is due to impaired miR24 and miR93 expression. Immunity 27: 123–134. doi:10.1016/j.immuni.2007.05.014

Padroni G, Bikaki M, Novakovic M, Wolter AC, Rüdisser SH, Gossert AD, Leitner A, Allain FHT. 2022. A hybrid structure determination approach to investigate the druggability of the nucleocapsid protein of SARS-CoV-2. Nucleic Acids Res 51: 4555–4571. doi:10.1093/nar/gkad195

Panda M, Kalita E, Singh S, Kumar K, Rao A, Prajapati VK. 2022. MiRNA-SARS-CoV-2 dialogue and prospective anti-COVID-19 therapies. Life Sci 305: 120761. doi:10.1016/j.lfs.2022.120761

Piotto M, Saudek V, Sklenár V. 1992. Gradient-tailored excitation for single-quantum NMR spectroscopy of aqueous solutions. J Biomol NMR 2: 661–665. doi:10.1007/BF02192855

Rambaut A, Posada D, Crandall KA, Holmes EC. 2004. The causes and consequences of HIV evolution. Nat Rev Genet 5: 52–61. doi:10.1038/nrg1246

Rist MJ, Marino JP. 2002. Mechanism of nucleocapsid protein catalyzed structural isomerization of the dimerization initiation site of HIV-1. Biochemistry 41: 14762–14770. doi:10.1021/bi0267240

Robertson MP, Igel H, Baertsch R, Haussler D, Ares M, Scott WG. 2005. The structure of a rigorously conserved RNA element within the SARS virus genome. PLoS Biol 3: e5. doi:10.1371/journal.pbio.0030005

Shetty S, Kim S, Shimakami T, Lemon SM, Mihailescu M-R. 2010. Hepatitis C virus genomic RNA dimerization is mediated via a kissing complex intermediate. RNA 16: 913–925. doi:10.1261/rna.1960410

Shimakami T, Yamane D, Jangra RK, Kempf BJ, Spaniel C, Barton DJ, Lemon SM. 2012. Stabilization of hepatitis C virus RNA by an Ago2-miR-122 complex. Proc Natl Acad Sci 109: 941–946. doi:10.1073/pnas.1112263109

Skalsky RL, Cullen BR. 2010. Viruses, microRNAs, and host interactions. Annu Rev Microbiol 64: 123–141. doi:10.1146/annurev.micro.112408.134243

Soremekun OS, Omolabi KF, Soliman MES. 2020. Identification and classification of differentially expressed genes reveal potential molecular signature associated with SARS-CoV-2 infection in lung adenocarcinomal cells. Inform Med Unlocked 20: 100384. doi:10.1016/j.imu.2020.100384

Sun X, Li JM, Wartell RM. 2007. Conversion of stable RNA hairpin to a metastable dimer in frozen solution. RNA 13: 2277–2286. doi:10.1261/rna.433307

Telenti A, Hodcroft EB, Robertson DL. 2022. The evolution and biology of SARS-CoV-2 variants. Cold Spring Harb Perspect Med 12: a041390. doi:10.1101/cshperspect.a041390

Tengs T, Jonassen CM. 2016. Distribution and evolutionary history of the mobile genetic element s2m in coronaviruses. Diseases 4: 27. doi:10.3390/diseases4030027

Tengs T, Kristoffersen AB, Bachvaroff TR, Jonassen CM. 2013. A mobile genetic element with unknown function found in distantly related viruses. Virol J 10: 132. doi:10.1186/1743-422X-10-132

Terada Y, Matsui N, Noguchi K, Kuwata R, Shimoda H, Soma T, Mochizuki M, Maeda K. 2014. Emergence of pathogenic coronaviruses in cats by homologous recombination between feline and canine coronaviruses. PLoS ONE 9: e106534. doi:10.1371/journal.pone.0106534

Tian D, Sun Y, Zhou J, Ye Q. 2021. The global epidemic of the SARS-CoV-2 Delta variant, key spike mutations and immune escape. Front Immunol 12: 751778. doi:10.3389/fimmu.2021.751778

Torrent C, Bordet T, Darlix JL. 1994. Analytical study of rat retrotransposon VL30 RNA dimerization in vitro and packaging in murine leukemia virus. J Mol Biol 240: 434–444. doi:10.1006/jmbi.1994.1459

Trobaugh DW, Klimstra WB. 2017. MicroRNA regulation of RNA virus replication and pathogenesis. Trends Mol Med 23: 80–93. doi:10.1016/j.molmed.2016.11.003

Vial T, Descotes J. 1995. Immune-mediated side-effects of cytokines in humans. Toxicology 105: 31–57. doi:10.1016/0300-483X(95)03124-X

Wacker A, Weigand JE, Akabayov SR, Altincekic N, Bains JK, Banijamali E, Binas O, Castillo-Martinez J, Cetiner E, Ceylan B, et al. 2020. Secondary structure determination of conserved SARS-CoV-2 RNA elements by NMR spectroscopy. Nucleic Acids Res 48: 12415–12435. doi:10.1093/nar/gkaa1013

Wu F, Zhao S, Yu B, Chen Y-M, Wang W, Song Z-G, Hu Y, Tao Z-W, Tian J-H, Pei Y-Y, et al. 2020. A new coronavirus associated with human respiratory disease in China. Nature 579: 265–269. doi:10.1038/s41586-020-2008-3

Yan R, Zhang Y, Li Y, Xia L, Guo Y, Zhou Q. 2020. Structural basis for the recognition of SARS-CoV-2 by full-length human ACE2. Science 367: 1444–1448. doi:10.1126/science.abb2762

Yang Y, Shen C, Li J, Yuan J, Wei J, Huang F, Wang F, Li G, Li Y, Xing L, et al. 2020. Plasma IP-10 and MCP-3 levels are highly associated with disease severity and predict the progression of COVID-19. J Allergy Clin Immunol 146: 119–127.e4. doi:10.1016/j.jaci.2020.04.027

Yaniv K, Ozer E, Shagan M, Paitan Y, Granek R, Kushmaro A. 2022. Managing an evolving pandemic: cryptic circulation of the Delta variant during the Omicron rise. Sci Total Environ 836: 155599. doi:10.1016/j.scitotenv.2022.155599

Yeh T, Contreras GP. 2020. Emerging viral mutants in Australia suggest RNA recombination event in the SARS-CoV-2 genome. Med J Aust 13: 44–44.e1. doi:10.5694/mja2.50657

Zarei Ghobadi M, Emamzadeh R, Teymoori-Rad M, Afsaneh E. 2022. Exploration of blood–derived coding and non-coding RNA diagnostic immunological panels for COVID-19 through a co-expressed-based machine learning procedure. Front Immunol 13: 1001070. doi:10.3389/fimmu.2022.1001070

Zhao J, Qiu J, Aryal S, Hackett JL, Wang J. 2020. The RNA architecture of the SARS-CoV-2 3′-untranslated region. Viruses 12: E1473. doi:10.3390/v12121473

Zúñiga S, Sola I, Moreno JL, Sabella P, Plana-Durán J, Enjuanes L. 2007. Coronavirus nucleocapsid protein is an RNA chaperone. Virology 357: 215–227. doi:10.1016/j.virol.2006.07.046

See the following page for Meet the First Author

MEET THE FIRST AUTHOR

Caylee L. Cunningham

Meet the First Author(s) is an editorial feature within RNA, in which the first author(s) of research-based papers in each issue have the opportunity to introduce themselves and their work to readers of RNA and the RNA research community. Caylee L. Cunningham is the first author of this paper, "Effect of the SARS-CoV-2 Delta-associated G15U mutation on the s2m element dimerization and its interactions with miR-1307-3p." She is a fifth-year PhD student in the Department of Chemistry and Biochemistry at Duquesne University, and a member of the Mihailescu research group where the primary research focus is biophysical chemistry. Specifically, her focus is on the relationship between nucleic acid structure and function studies as well as characterizing the interactions between nucleic acids and proteins with implications in viral and neurodegenerative diseases. She received her undergraduate degree in Biochemistry & Molecular Biology from the College of Wooster in 2019.

What are the major results described in your paper and how do they impact this branch of the field?

We have revealed that there is a 99% correlation of a G to U mutation at position 15 within the highly conserved s2m of the Delta variant of SARS-CoV-2. Our previous work revealed that this stem–loop element can dimerize and interact with host miR-1307-3p. However, as this G15U mutation was introduced to the s2m, it significantly decreased the ability of miR-1307-3p to bind. Considering the almost total elimination of the s2m in the Omicron variant, these results may suggest a stepwise elimination of miR binding for the sake of decreased disease severity and viral longevity.

What led you to study RNA or this aspect of RNA science?

The study of RNA has always been interesting to me partly because of its broad range of functions and the hypothesis that RNA predated DNA and proteins. Knowing some of these roles makes studying RNA so versatile and exciting—there is always something new and translational. The fundamentals of nucleic acids always came easier to me than other areas of biochemistry, and that is probably because I was truly interested in it. However, on a less scientific level, what led me to pursue this work specifically were the people. I remember going through the graduate school application process and being told numerous times to "choose the mentor, not necessarily the project," and that is truly some of the best advice. I would not be here if I did not love my mentors, both former and fellow graduate students, my PI, and the undergraduate group members. I am fortunate to work with an excellent and supportive group that keeps me engaged and continuously inspired to question new things in the laboratory. Obviously, loving the work helps considerably, but you need to be in the right place to grow too.

During the course of these experiments, were there any surprising results or particular difficulties that altered your thinking and subsequent focus?

Like most projects, there are always some stumbling points. However, one of the more surprising things to arise in this project was seeing the decrease in miR-1307-3p binding. We previously believed that the virus would selectively want to hijack this host miR, as this has been shown to be beneficial to the viral life cycle in several other viruses. As we were collecting this data, we continued our bioinformatics work and showed a strong correlation of the Omicron variant with a large s2m deletion, which eliminated the binding sites entirely. Although this could be the result of hitchhiking to a more positively selected mutation elsewhere in the virus, it did steer us to alter our thinking that SARS-CoV-2 could be adapting to evade the immune response of the host through decreased miR-1307-3p interaction.

What are some of the landmark moments that provoked your interest in science or your development as a scientist?

I always enjoyed science and participating in new things, but I remember the first time something actually provoked my interest in science was when I got my first pH color changing lipstick as a kid. It was captivating, and I made sure to show it off to everyone I knew (several of which did not share my middle school level of enthusiasm). Since then, I would say a true landmark memory for me was a few years later when I was administered a very recently FDA-approved drug. Although it did not mean much to me then, years later I now find it so fascinating to think about how differently my life would be had it been approved even one year later. Although these were not the only occurrences that inspired me to pursue science, I am forever thankful for and amazed by the work scientists across the board are doing.

If you were able to give one piece of advice to your younger self, what would that be?

Never stop networking. On numerous occasions I have been introduced to an area of science simply by meeting someone new. There are fields of study that I never would have guessed existed in the past, and some of these have truly changed my way of thinking about project goals. Also, it is always great to add people to your corner. A strong support system is unmatched.

What are your subsequent near- or long-term career plans?

With graduation fast approaching, I have started to narrow down my interests, which has been both daunting and gratifying. Although my options are not solidified yet, I do know that something I am proud of and have quite enjoyed during my graduate studies has been outreach, so I hope wherever I land in the future still enables me to build and maintain strong connections with others from all scientific backgrounds.

Effect of the SARS-CoV-2 Delta-associated G15U mutation on the s2m element dimerization and its interactions with miR-1307-3p

Caylee L. Cunningham, Caleb J. Frye, Joseph A. Makowski, et al.

RNA 2023 29: 1754-1771 originally published online August 21, 2023
Access the most recent version at doi:10.1261/rna.079627.123